Microbiology Spectrum

| Virology | Research Article

Marburg virus exploits the Rab11-mediated endocytic pathway in viral-particle production

Wakako Furuyama,[1] Kento Yamada,[1] Miako Sakaguchi,[2] Andrea Marzi,[3] Asuka Nanbo[1]

AUTHOR AFFILIATIONS See affiliation list on p. 20.

ABSTRACT Filoviruses produce viral particles with characteristic filamentous morphology. The major viral matrix protein, VP40, is trafficked to the plasma membrane and promotes viral particle formation and subsequent viral egress. In the present study, we assessed the role of the small GTPase Rab11-mediated endocytic pathway in Marburg virus (MARV) particle formation and budding. Although Rab11 was predominantly localized in the perinuclear region, it exhibited a more diffuse distribution in the cytoplasm of cells transiently expressing MARV VP40. Rab11 was incorporated into MARV-like particles. Expression of the dominant-negative form of Rab11 and knockdown of Rab11 decreased the amount of VP40 fractions in the cell periphery. Moreover, downregulation of Rab11 moderately reduced the release of MARV-like particles and authentic MARV. We further demonstrated that VP40 induces the distribution of the microtubule network toward the cell periphery, which was partly associated with Rab11. Depolymerization of microtubules reduced the accumulation of VP40 in the cell periphery along with viral particle formation. VP40 physically interacted with α-tubulin, a major component of microtubules, but not with Rab11. Taken together, these results suggested that VP40 partly interacts with microtubules and facilitates their distribution toward the cell periphery, leading to the trafficking of transiently tethering Rab11-positive vesicles toward the cell surface. As we previously demonstrated the role of Rab11 in the formation of Ebola virus particles, the results here suggest that filoviruses in general exploit the vesicle-trafficking machinery for proper virus-particle formation and subsequent egress. These pathways may be a potential target for the development of pan-filovirus therapeutics.

IMPORTANCE Filoviruses, including Marburg and Ebola viruses, produce distinct filamentous viral particles. Although it is well known that the major viral matrix protein of these viruses, VP40, is trafficked to the cell surface and promotes viral particle production, details regarding the associated molecular mechanisms remain unclear. To address this knowledge gap, we investigated the role of the small GTPase Rab11-mediated endocytic pathway in this process. Our findings revealed that Marburg virus exploits the Rab11-mediated vesicle-trafficking pathway for the release of virus-like particles and authentic virions in a microtubule network-dependent manner. Previous findings demonstrated that Rab11 is also involved in Ebola virus-particle production. Taken together, these data suggest that filoviruses, in general, may hijack the microtubule-dependent vesicle-trafficking machinery for productive replication. Therefore, this pathway presents as a potential target for the development of pan-filovirus therapeutics.

KEYWORDS Marburg virus, virus-particle formation, virus egress, virus-like particles, Rab11, VP40, microtubules

Marburg virus (MARV), a member of the family *Filoviridae*, causes sporadic outbreaks of Marburg virus disease (MVD), formerly known as Marburg hemorrhagic fever.

Editor Leiliang Zhang, Shandong First Medical University, Jinan, Shandong, China

Address correspondence to Asuka Nanbo, nanboa@nagasaki-u.ac.jp.

Wakako Furuyama and Kento Yamada contributed equally to this article. The author order was determined in order of increasing seniority.

The authors declare no conflict of interest.

See the funding table on p. 20.

Received 12 March 2024
Accepted 10 June 2024
Published 30 July 2024

MVD is a severe and often fatal disease with a mortality rate of up to 88% in humans (1). Currently, neither specific vaccines nor therapeutics are approved for the treatment and prevention of MVD (2, 3), although the potential effectiveness of vaccines and therapeutics have been demonstrated in animal models (4).

MARV and Ebola virus (EBOV) encode seven structural genes in their single-stranded negative-sense RNA genomes that assemble to yield filamentous viral particles (5). The virus-encoded major matrix protein VP40 self-assembles to form virus-like particles (VLPs), which resemble the morphology of authentic viruses and are released from the cell surface even when VP40 is expressed by itself (6–9). While EBOV VP40 predominantly targets the plasma membrane (PM) as a site for VLP formation and release, MARV VP40 accumulates in multivesicular bodies in the cytoplasm in addition to the PM. VLP-positive multivesicular bodies are enriched at the PM for subsequent budding of MARV particles and VLPs (10–12).

The molecular mechanisms underlying the VP40-mediated release of filovirus particles have been intensively characterized. MARV and EBOV VP40 contain highly conserved late (L) domains (PPxY), and it has been revealed that various host factors interact with this motif via their WW domain and positively or negatively regulate this process (13). Members of the HECT family of E3 ubiquitin ligases, such as Nedd4 (14, 15), Itch (16), and WWP1 (17), and members of the endosomal sorting complex required for transport (ESCRT) pathway are hijacked by VP40 to facilitate filovirus egress and the release of VLPs (9, 15–18). Moreover, recent studies identified several host factors, including BAG3 (19, 20), YAP/TAZ (21, 22), and WWOX (23, 24), that interact with the VP40 L-domain and negatively regulate budding.

Several host proteins have also been identified as key factors in VP40 trafficking to the PM. For example, a Ras GAP-related actin-binding scaffolding protein, IQGAP1 (25), a component of the host COPII vesicular transport system, Sec24C (26), and a microtubule network (27) appear to be responsible for the intracellular transport of VP40 to the budding site. However, a comprehensive understanding of the underlying molecular mechanisms is lacking.

Growing evidence suggests that various viruses exploit the Rab11-mediated endocytic pathway during their assembly process by trafficking viral components to their egress sites for incorporation into virions (28). Rab11 is one of the most well-characterized small GTPases and, as a member of the Rab family, predominantly distributed in recycling endosomes and post-Golgi vesicles (29–32). Rab11 is indispensable for the regulation of cargo recycling through recycling and secretory vesicles (29, 33) and other cellular processes, including cell migration (34), ciliogenesis (35), and phagocytosis (36).

Influenza A virus (IAV), Sendai virus (37, 38), and human parainfluenza virus type I (38) exploit the Rab11-mediated pathway for viral ribonucleoprotein transport toward the egress sites. The viral structural proteins of human immunodeficiency virus 1 (39) and Nipah virus (40) are also transported to the PM via Rab11-positive vesicles for incorporation into virions. Moreover, a potential role for the Rab11-dependent pathway in viral egress has been suggested for various RNA viruses, including the respiratory syncytial virus (RSV) (41, 42), filamentous IAV (43), Mason-Pfizer monkey virus (28, 44), Jaagsiekte sheep retrovirus (45), and hepatitis C virus (46).

Only a few studies have demonstrated the role of the Rab11-mediated pathway in the filovirus life cycle. Liquid chromatography-linked tandem mass spectroscopy revealed that the Rab11b isoform is incorporated into authentic filovirus virions (47, 48). Our group has clarified the critical role of the Rab11-dependent vesicle traffic pathway in the VP40-mediated release of Ebola VLPs (49).

This study assessed the role of the Rab11-mediated pathway in the MARV replication cycle. We found that the transient expression of MARV VP40 promoted the diffuse cytoplasmic distribution of Rab11, which is normally localized in the perinuclear region. We also observed that Rab11 was incorporated into Marburg VLPs. The expression of a dominant-negative form and knockdown of Rab11 decreased VP40 distribution to the cell periphery. Moreover, we demonstrated that the release of Marburg

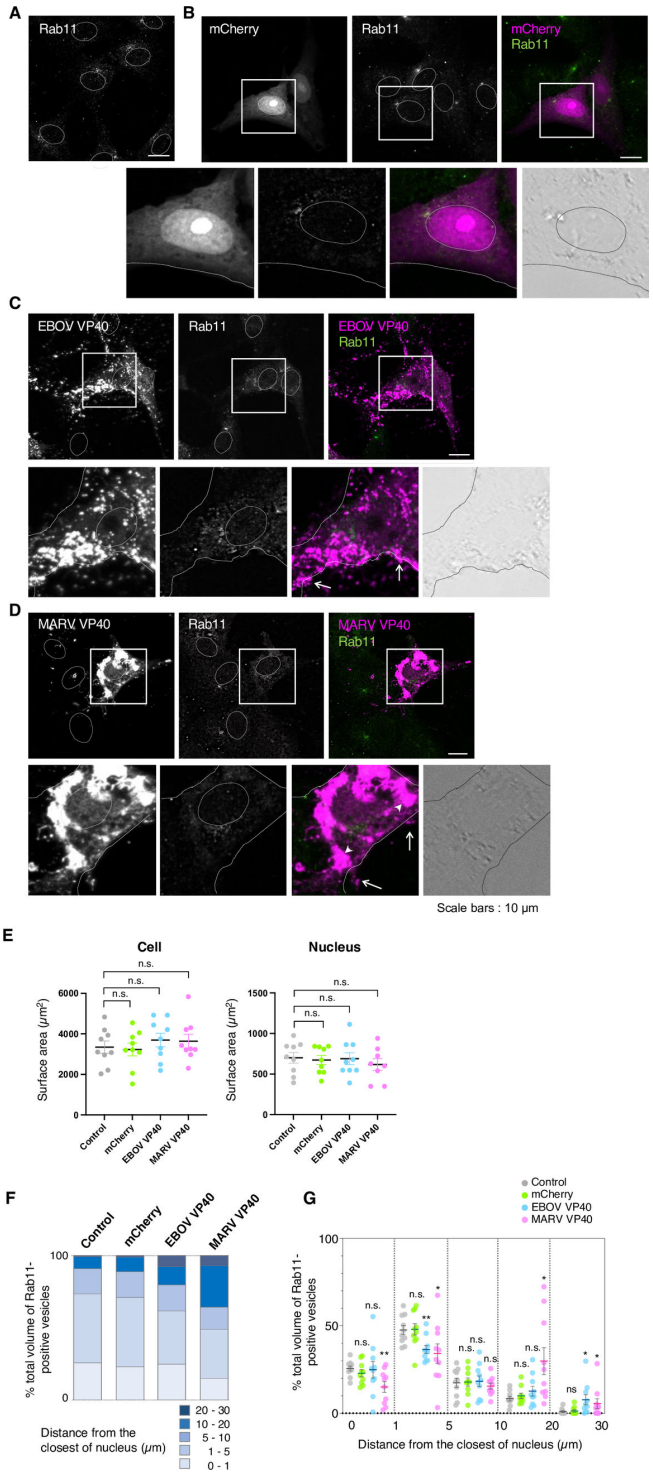

FIG 1 Filovirus VP40 induced a dispersed distribution of Rab11. (A–D) Effect of filovirus VP40 expression on the intracellular distribution of endogenous Rab11. Vero-E6 cells were transfected with the expression plasmids for (B) mCherry, (C) Ebola virus (EBOV) VP40, and (D) Marburg virus (MARV) VP40. (A) A backbone plasmid was transfected as a control. At 24 h post-transfection, the cells were harvested, and the subcellular distribution of VP40 and Rab11 was analyzed using immunofluorescence staining. Ten cells in three to five fields were analyzed; the representative images are shown. The nuclei were counterstained with Hoechst 33342, and the dotted lines indicate their outlines. Insets show the box area; cell peripheries were determined by phase contrast images and shown in lines; arrows show filamentous

(Continued on next page)

FIG 1 (Continued)

structures on the cell surface; arrowheads indicate the intracellular patched structures; scale bars: 10 µm. (E–G) Quantification of the intracellular distribution of Rab11 upon expression of filovirus VP40. (E) The surface area (μm^2) of the cell and the nucleus were measured using IMARIS imaging software. (F) The distance (µm) between Rab11-positive vesicles and the closest nucleus and their volumes in single cells were measured using the IMARIS imaging software. The ratio of the total volume of Rab11-positive signals distributed in the indicated regions in single cells was measured. Ten cells were analyzed; the results are shown as the mean ± SD. (G) Summary of the % total volume of Rab11-positive vesicles detected at the indicated distance from the closest nucleus of the analyzed cells. n.s.; not significance, *, $P < 0.05$; **, $P < 0.01$ versus respective control (Student's *t* test).

VLPs and progeny infectious MARV was moderately reduced upon downregulation of Rab11. We further demonstrated that VP40 modulates the distribution of microtubules toward the cell periphery, which was often associated with Rab11. Depolymerization of microtubules reduced the accumulation of VP40 in the cell periphery along with viral-particle formation. VP40 physically interacted with α-tubulin, a major component of microtubules, but not with Rab11. Our findings suggest that MARV VP40 interacts with microtubules and facilitates their distribution toward the cell periphery, leading to the trafficking of transiently tethering Rab11-positive vesicles toward the cell surface and the subsequent release of virus particles to establish efficient viral egress.

RESULTS

MARV VP40 induces a dispersed distribution of Rab11

First, we investigated the effect of transiently expressed filovirus VP40 on the subcellular localization of Rab11. In plasmid-transfected and mCherry-expressing cells, Rab11 was predominantly distributed in the perinuclear region (Fig. 1A and B), suggesting its involvement in recycling endosomes and post-Golgi vesicles (30). Then, we elucidated the intracellular distribution of transiently expressed filovirus VP40. MARV and EBOV VP40 were similarly distributed in multiple subcellular compartments, such as the cytoplasm, nucleus, and PM, along with filamentous structures from the cell surface (50) (Fig. 1C and D; insets, arrows). In accordance with previous findings (11, 12), we observed that MARV VP40 showed large aggregates distributed in the cytoplasm (Fig. 1D, insets, arrowhead), which was not observed for EBOV VP40 (Fig. 1C). Co-immunofluorescence staining revealed that the expression of both VP40s induced a diffuse distribution of Rab11 throughout the cytoplasm (Fig. 1C and D; insets). However, no efficient co-localization of filovirus VP40 with Rab11 was observed.

We measured the distance between Rab11-positive vesicles and the closest nucleus and the ratio of the total volume of each Rab11-positive signal observed in the indicated regions outward from the nucleus. We confirmed that the overexpression of mCherry and filovirus VP40 did not affect the surface area of cell bodies and nucleus (Fig. 1E). Ratio of Rab11 that was distributed closer to the periphery of cells increased by expression of EBOV or MARV VP40 (Fig. 1F and G). For example, while 0.9% or 1.3% of the total volume of the Rab11-positive signal was distributed in the region more than 20 µm away from the nucleus of the control or mCherry-expressing cells, respectively, 7.7% or 7.5% of the Rab11-positive signal fraction was distributed in the same region of the cells expressing EBOV or MARV VP40, respectively (Fig. 1F and G). Modulation of Rab11 distribution was not observed in cells transiently expressing the MARV glycoprotein (GP; Fig. 2A) or nucleoprotein (NP; Fig. 2B), which are also major components of viral particles. Moreover, neither GP nor NP was shown to be co-localized with Rab11 (Fig. 2). We also confirmed the effect of the MARV GP and NP on the distribution of Rab11-positive vesicles by measuring the distance between Rab11 signals and the closest nucleus (Fig. 2C through E).

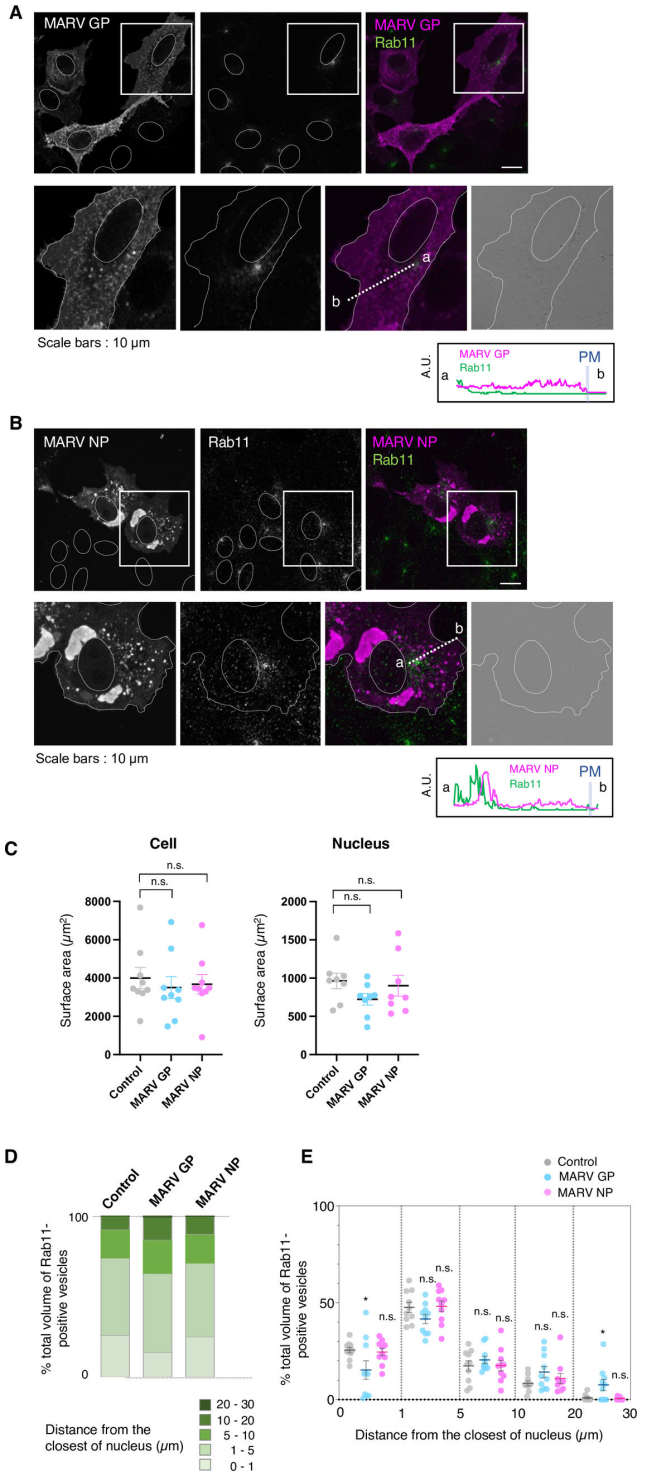

FIG 2 Effect of MARV GP and NP on distribution of Rab11. (A and B) Effect of MARV GP and NP expression on the intracellular distribution of endogenous Rab11. Vero-E6 cells were transfected with expression plasmids for (A) MARV glycoprotein (GP) or (B) MARV nucleoprotein (NP). At 24 h post-transfection, the cells were harvested, and the subcellular distribution of GP or NP, and Rab11 was analyzed using immunofluorescence staining. Ten cells in three to five fields were analyzed; the representative images are shown. The nuclei were counterstained with Hoechst 33342, and the dotted lines indicate their outlines. Insets show the box area; cell peripheries were determined by phase contrast images and shown in lines. The plots indicate individual fluorescence intensities along each line. The location of the PM is

(Continued on next page)

FIG 2 (Continued)

shown in pale blue bars. A.U.; arbitrary unit. Scale bars: 10 µm. (C–E) Quantification of the intracellular distribution of Rab11 upon expression of MARV GP and NP. (C) The surface area (μm^2) of the cell and the nucleus were measured using IMARIS imaging software. (D) The distance (µm) between Rab11-positive vesicles and the closest nucleus and their volumes in single cells were measured using IMARIS imaging software. The ratio of the total volume of Rab11-positive signals distributed in the indicated regions in single cells was measured. Ten cells were analyzed; the results are shown as the mean ± SD. (E) Summary of the % total volume of Rab11-positive vesicles detected at the indicated distance from the closest nucleus of the analyzed cells. n.s.; not significance, *, $P < 0.05$; versus respective control (Student's *t* test).

Rab11 is incorporated in MARV VLPs

We examined the incorporation of Rab11 into MARV particles using two independent analyses. We generated Marburg VLPs by co-expressing VP40 along with the viral GP and NP in Expi293F cells, purified them by ultracentrifugation, and confirmed their morphology by negative-staining electron microscopy (Fig. 3A). Membranous objects were not observed in the control fractions, which were obtained from the culture supernatants of the backbone plasmid-transfected cells (Fig. 3A). Western blotting analysis revealed that VP40 and Rab11 were present in the purified VLP fractions (Fig. 3B), indicating that Rab11 is incorporated into MARV particles. We further confirmed the incorporation of Rab11 into Marburg VLPs using a protease protection assay (49, 51). Purified VLPs were treated with or without Triton X-100 at room temperature for 10 min and further incubated at the same condition in the presence or absence of trypsin, followed by

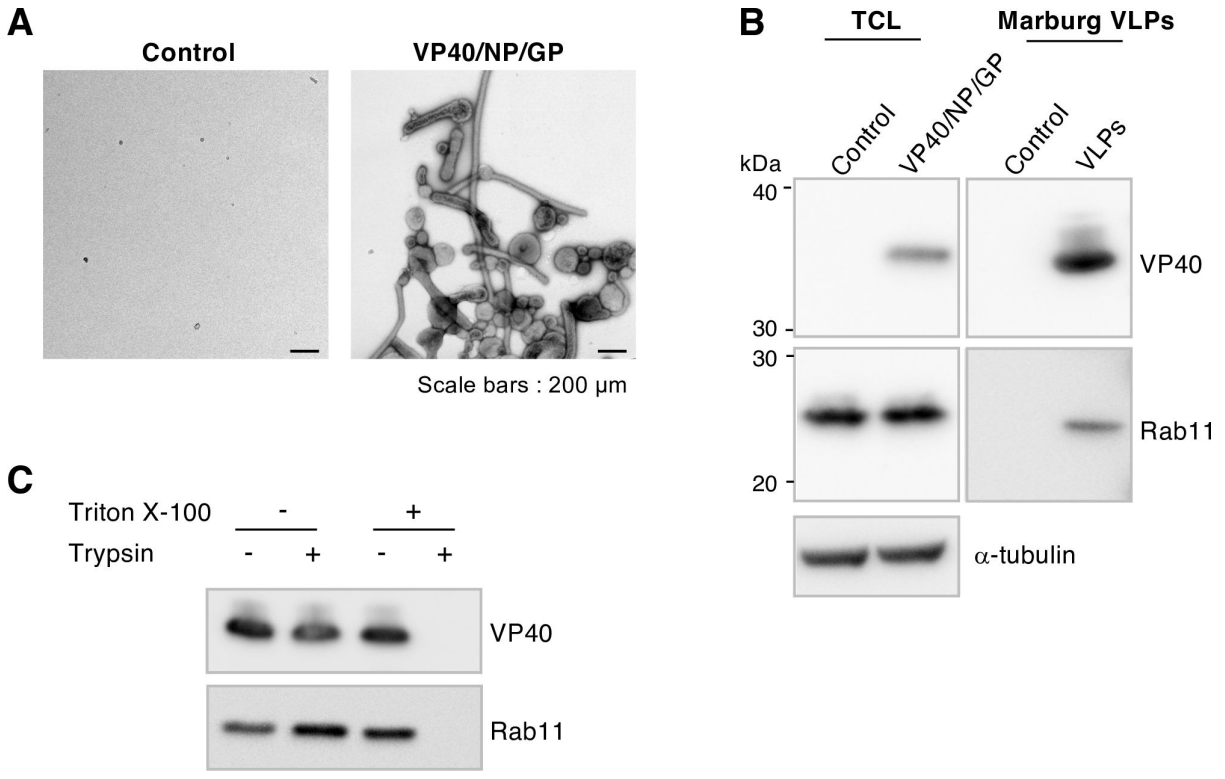

FIG 3 Rab11 is incorporated into Marburg virus-like particles (VLPs). (A) Electron micrograph of Marburg VLPs. Marburg VLPs (right) were subjected to negative staining. The fraction obtained from cell supernatant from the cells transfected with a backbone plasmid was applied as a control (left). Scale bars: 200 µm. (B) Determination of Rab11 incorporation in Marburg VLPs by western blotting. Expi293F cells were transfected with expression plasmids for MARV VP40, GP, and NP. At 48 h.p.t., VLPs released into the culture medium were purified by ultracentrifugation. Total cell lysates (TCLs) and VLPs were subjected to western blotting using antibodies against VP40 and Rab11. The cells transfected with a backbone plasmid were used as a control. (C) Protease protection assay. VLPs were treated with or without Triton X-100 and further treated with or without trypsin, followed by western blotting analysis with the antibodies for MARV VP40 or Rab11. The experiment was performed three times independently, and the representative blot is shown.

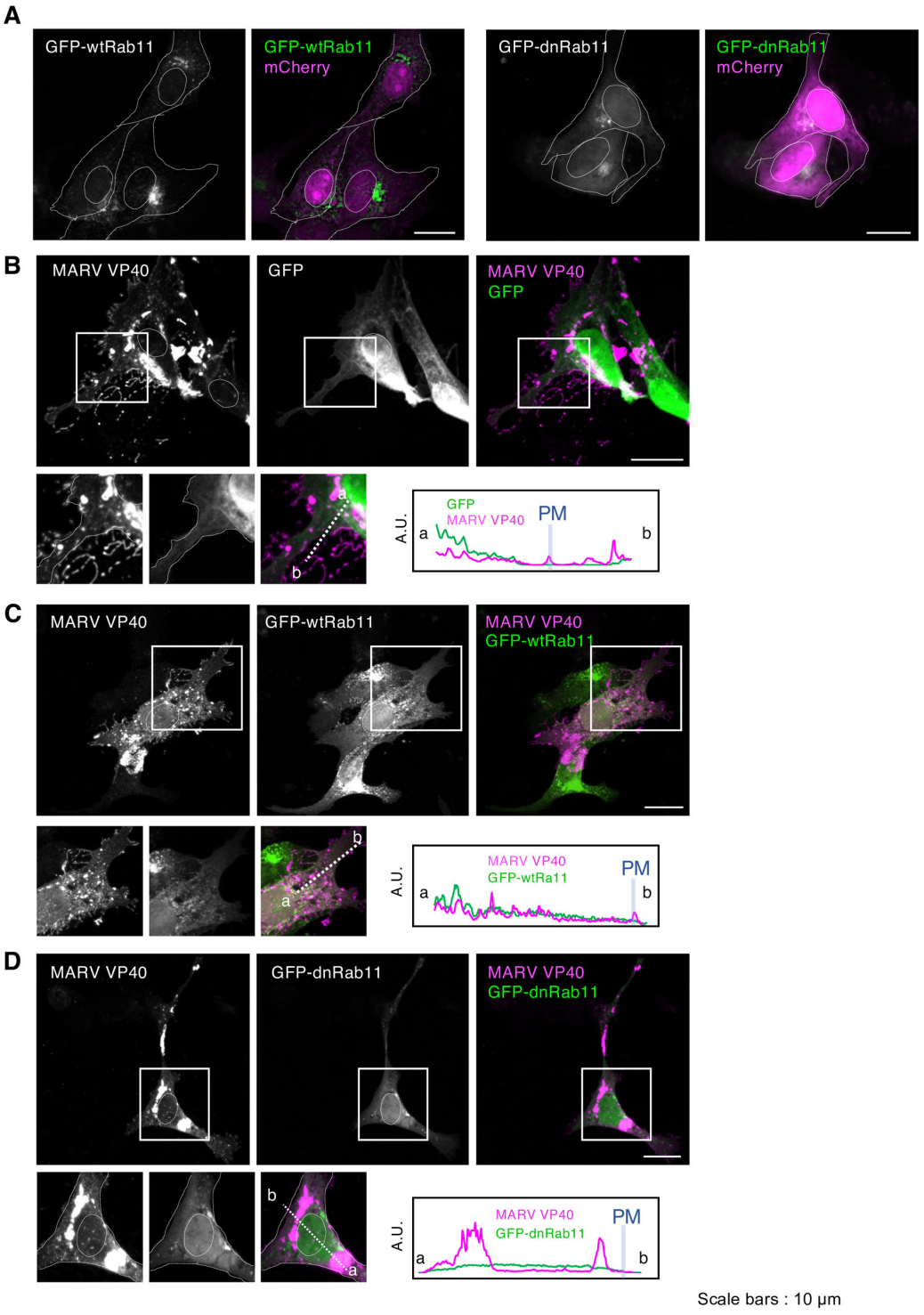

FIG 4 Effect of a dominant-negative form of Rab11 on the distribution of VP40. (A–D) Effect of the dominant-negative form of Rab11 on the distribution of VP40. Vero-E6 cells grown on coverslips were transfected with expression plasmids for GFP (B), GFP-wtRab11 (C) or -dnRab11 (D), and VP40. As a control, cells were co-expressed with mCherry and GFP-wtRab11 (A), or -dnRab11. At 24 h.p.t., the cells were harvested, and the subcellular distribution of VP40 and GFP-Rab11 derivatives was analyzed using immunofluorescence staining. Ten cells in 5–10 fields per sample were analyzed; the representative images are shown. The insets show the boxed areas. The nuclei were counterstained with Hoechst 33342, and the dotted lines indicate their outlines. Insets show the box area; cell peripheries were determined by GFP signals and shown in dotted lines. The plots indicate individual fluorescence intensities along each line. The location of the PM is shown in pale blue bars. A.U.; arbitrary unit. Scale bars: 10 μm.

western blotting analysis using antibodies against VP40 and Rab11. While both VP40 and Rab11 were similarly detected in Marburg VLPs treated with trypsin or Triton X-100 alone, trypsinization of Triton X-100-treated VLPs abolished the signals of VP40 and Rab11 (Fig. 3C), further confirming the incorporation of Rab11 in VLPs.

Effect of the dominant-negative form of Rab11 on VP40 distribution and subsequent Marburg VLP formation

Because MARV VP40 modulated the intracellular distribution of Rab11 (Fig. 1) and Rab11 was incorporated into Marburg VLPs (Fig. 3), we further assessed the role of Rab11 in VP40-mediated MARV particle formation. We transiently expressed the GFP-fused wild-type (GFP-wtRab11) or the dominant-negative form of Rab11 (GFP-dnRab11) and MARV VP40 in Vero-E6 cells. The GFP-dnRab11 has an amino-acid substitution (S25N) and preferentially keeps the GDP-bound status, inhibiting the recycling of cargo from the intracellular recycling compartments to the cell surface (30, 52, 53). The effect of the Rab11 derivatives on the distribution of VP40 was examined using immunofluorescence staining. When GFP-wtRab11 was co-expressed with mCherry, it exhibited a predominant distribution in the perinuclear region (Fig. 4A, left) similar to endogenous Rab11 (Fig. 1A). Consistent with the results for endogenous Rab11 (Fig. 1D), efficient co-localization of GFP-wtRab11 with VP40 was not observed.

In contrast, GFP-wtRab11 was distributed diffusely throughout the cytoplasm of MARV VP40-expressing cells. Similar to that of the cells expressing GFP (Fig. 4B, inset and line scan), a fraction of VP40 was distributed to the periphery of the cells with intense clusters (Fig. 4C, inset and line scan). In contrast, GFP-dnRab11 was diffusely distributed in the cytoplasm and partially formed perinuclear clusters in both VP40-positive (Fig. 4D) and -negative (Fig. 4A, right) cells. Upon GFP-dnRab11 expression, VP40 formed large aggregates in the cytoplasm without an intense distribution at the PM (Fig. 4D).

Rab11 contributes to the distribution of VP40 in the PM and subsequent Marburg VLP formation

Next, we assessed the role of Rab11 in the trafficking of VP40 to the PM by knocking down endogenous Rab11 using siRNAs targeting two Rab11 isoforms: Rab11a (54) and Rab11b (55). These two isoforms share 89% amino acid sequence homology and contribute to vesicle-mediated cargo recycling toward the cell surface. Rab11a and Rab11b show ubiquitous and tissue-specific expression, respectively. We treated Vero-E6 cells with siRNAs against the two Rab11 isoforms and confirmed Rab11 downregulation using western blotting (Fig. 5A and B). We then assessed the effect of Rab11 knockdown on MARV VP40 distribution. In both untreated and control siRNA-treated cells, VP40 similarly formed clusters in the cytoplasm and cell periphery and thread-like structures in the PM (Fig. 5C and D, insets, line scans). In contrast, cells in which Rab11 isoforms were downregulated showed the reduction of the formation of VP40-positive clusters at the PM and filamentous structures from the cell periphery (Fig. 5E, inset, line scan). We further determined the effect of Rab11 downregulation on VP40-mediated Marburg VLP formation. HEK293 cells were transfected with siRNAs targeting Rab11 isoforms. At 72 h post-transfection (h.p.t.), while a minimal effect of the knockdown of Rab11 isoforms on the expression of the three MARV structural proteins was confirmed (Fig. 6A and B), expression plasmids for VP40, NP, and GP were transfected to produce VLPs. Rab11 downregulation resulted in a 30% reduction in the formation of Marburg VLPs (Fig. 6C and D).

Effect of Rab11 downregulation on viral particle production in MARV-infected cells

We assessed the effects of Rab11 knockdown on viral particle production in MARV-infected cells. HEK293 and Vero-E6 cells were treated with siRNAs for Rab11, and the knockdown efficiency was confirmed using western blotting (Fig. 7A and B). The siRNA-treated cells were infected with MARV at a multiplicity of infection (MOI) of 0.01.

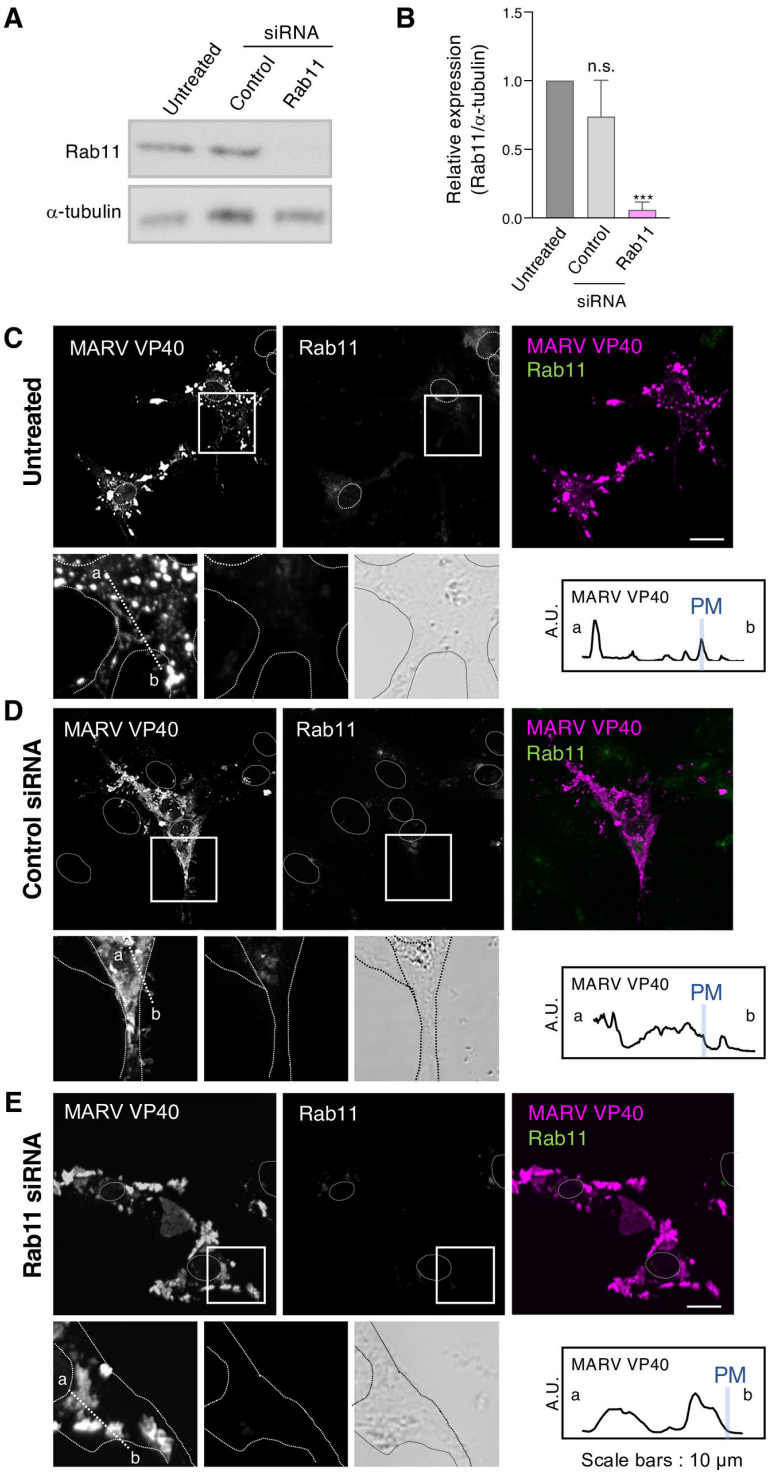

FIG 5 Downregulation of Rab11 decreased the amount of VP40 fractions distributed to the PM. (A) Downregulation of Rab11 by siRNA treatment. Vero-E6 cells were transfected with or without control siRNAs or siRNAs against Rab11a and Rab11b. At 72 h.p.t., Rab11 expression in siRNA-treated cells was analyzed by western blotting. The experiment was performed three times independently, and the representative blot is shown. (B) The intensity of the band's correspondence to each protein was quantified, and the results are shown as mean ± SD. n.s., not significant; ***, $P < 0.001$ versus respective control (Student's *t* test). (C–E) Analysis of the subcellular distribution of VP40 in the siRNA-treated cells. (C) siRNA-untreated cells are shown as controls. Seventy-two hours after transfection of (D) control siRNAs

(Continued on next page)

FIG 5 (Continued)

or (E) siRNAs for Rab11, Vero-E6 cells were further transfected with the expression plasmid of VP40. At 48 h.p.t., the subcellular distribution of VP40 and Rab11 was analyzed using immunofluorescence staining. Ten cells in 5–10 fields per sample were analyzed; the representative images are shown. The nuclei were counterstained with Hoechst 33342, and the dotted lines indicate their outlines. The insets show the boxed areas. The plots indicate the individual fluorescence intensity along each of the periphery of individual cells was determined by the phase contrast images and shown in corresponding dotted lines. The location of the PM is shown in pale blue bars. A.U.; arbitrary unit. Scale bars in the large panels: 10 µm.

Two days post-infection, the effect of Rab11 downregulation on MARV infection was determined using titration. We observed a minimal effect of Rab11 knockdown on MARV infection in both cell types (Fig. 7C). To elucidate the effect of Rab11 downregulation on the production of progeny MARV, we infected siRNA-treated cells with MARV at an MOI of 0.01, harvested supernatants at various times during incubation, and determined the MARV titer. We found that the production of infectious viral particles was indeed moderately reduced in both cell types (Fig. 7D and E), indicating that Rab11 is involved in MARV particle formation and subsequent viral egress.

VP40 exploits the microtubule network for self and tethering Rab11-positive vesicle trafficking toward the cell surface for efficient VLP formation

Rab11 links the vesicles to the cytoskeleton by interacting with specific motor proteins and mediating active and directed vesicle transport along microtubules or actin filaments (56). We examined the distribution of microtubules in the cells expressing VP40 using immunofluorescence staining. In control cells, the microtubule network was visualized to be extended from the microtubule organizing center in the perinuclear region (Fig. 8A). In contrast, VP40-positive cells exhibited the decrease of polarized distribution in the perinuclear region and distribution of microtubule network toward the cell periphery (Fig. 8A and B, insets, line scans). A fraction of VP40 appears to be co-localized with tubulin (Fig. 8B, inset, line scan). Treatment with nocodazole, a microtubule depolymerizer, resulted in the decrease of cluster formation of MARV VP40 at the cell periphery (Fig. 8C, inset, line scan). Nocodazole treatment also negatively affected the production of VLPs (Fig. 8D and E). The data suggest that VP40-induced microtubule network distribution toward the PM is likely involved in the transport of VP40 itself at the cell periphery and in VLP formation.

Because VP40 was not efficiently co-localized with diffusely distributed Rab11 (Fig. 1D), we next elucidated whether VP40-induced microtubule distribution toward the cell periphery is responsible for the dispersed distribution of tethering Rab11-positive vesicles. A previous study demonstrated that the fusion of the red-fluorescent protein to the N-terminus of MARV VP40 does not disrupt its functionality (57). Thus, Vero-E6 cells were transfected with expression plasmids for mCherry fused to the N-terminus of VP40 and VP40 in a 1:5 ratio. Expression of mCherry-VP40 also induced an increase in microtubule distribution toward the cell periphery (Fig. 8F and G, inset, line scans). The dispersed Rab11-positive vesicles were often detected adjacent to microtubules in mCherry-VP40-positive cells (Fig. 8G, inset). The intensity-based co-localization analysis indicated that approximately 40% of Rab11 signals were co-localized with α-tubulin in multiple cells.

Finally, we investigated the interaction of MARV VP40 and α-tubulin by immunoprecipitation. Transiently expressed VP40 was co-immunoprecipitated with α-tubulin (Fig. 9A) and its interaction was not disrupted in the presence of nocodazole (Fig. 9B), suggesting that VP40 associates with the depolymerized form of tubulin. Their physical interaction was also confirmed by the detection of α-tubulin in the precipitants using the anti-VP40 antibody (Fig. 9A and B). In contrast, no interaction was observed between co-expressed VP40 and GFP-fused Rab11 derivatives (Fig. 9C), which is consistent with the data of lack of efficient co-localization of VP40 with endogenous Rab11 (Fig. 1D). Taken together,

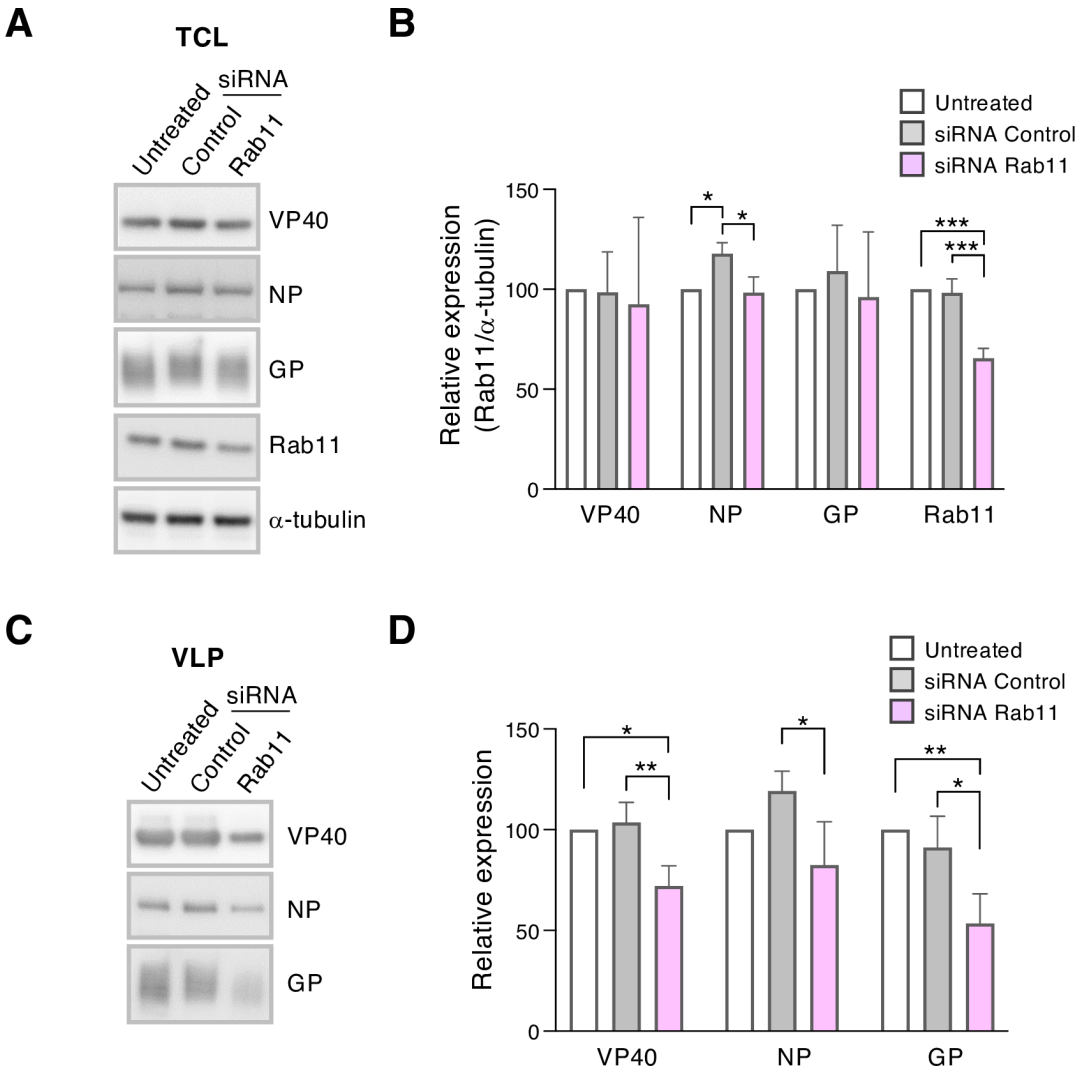

FIG 6 Effect of Rab11 downregulation on Marburg VLPs formation. (A) Downregulation of Rab11. HEK293 cells were transfected with siRNAs against Rab11a and Rab11b. At 72 h.p.t., the cells were transfected with the expression plasmids for MARV VP40, NP, and GP. At 48 h.p.t., the cells and culture medium were harvested. TCLs were subjected to western blotting with the antibodies against VP40, NP, GP, Rab11, or α-tubulin. (B) The intensity of the band's correspondence to VP40, NP, and GP was quantified and normalized with that of α-tubulin. (C) VLPs in the culture medium were purified by ultracentrifugation, and VLPs were subjected to western blotting with the antibodies against VP40, NP, or GP. (D) The intensity of the band's correspondence to each protein was quantified. The experiment was performed three times independently, and representative blots (A and C) and the mean ± SD are shown (B and D). *, $P < 0.05$; **, $P < 0.01$; ***, $P < 0.001$ versus respective control (one-way ANOVA).

these data suggest that VP40 associates with the microtubule network for trafficking of itself and tethering Rab11-positive vesicles toward the cell periphery, contributing to MARV particle formation.

DISCUSSION

In the present study, we demonstrated that the MARV VP40 exploits the microtubule-dependent trafficking of Rab11-positive vesicles to the PM for the release of MARV particles. Endogenous Rab11 was distributed more diffusely in the cytoplasm upon MARV VP40 expression (Fig. 1 and 2) and was subsequently incorporated into VLPs (Fig. 3). We also observed that blocking Rab11 function by either the expression of a dominant-negative form of Rab11 or knockdown of Rab11 by siRNA decreased the amount of VP40 distributed to the periphery of the cells (Fig. 4 and 5). We further

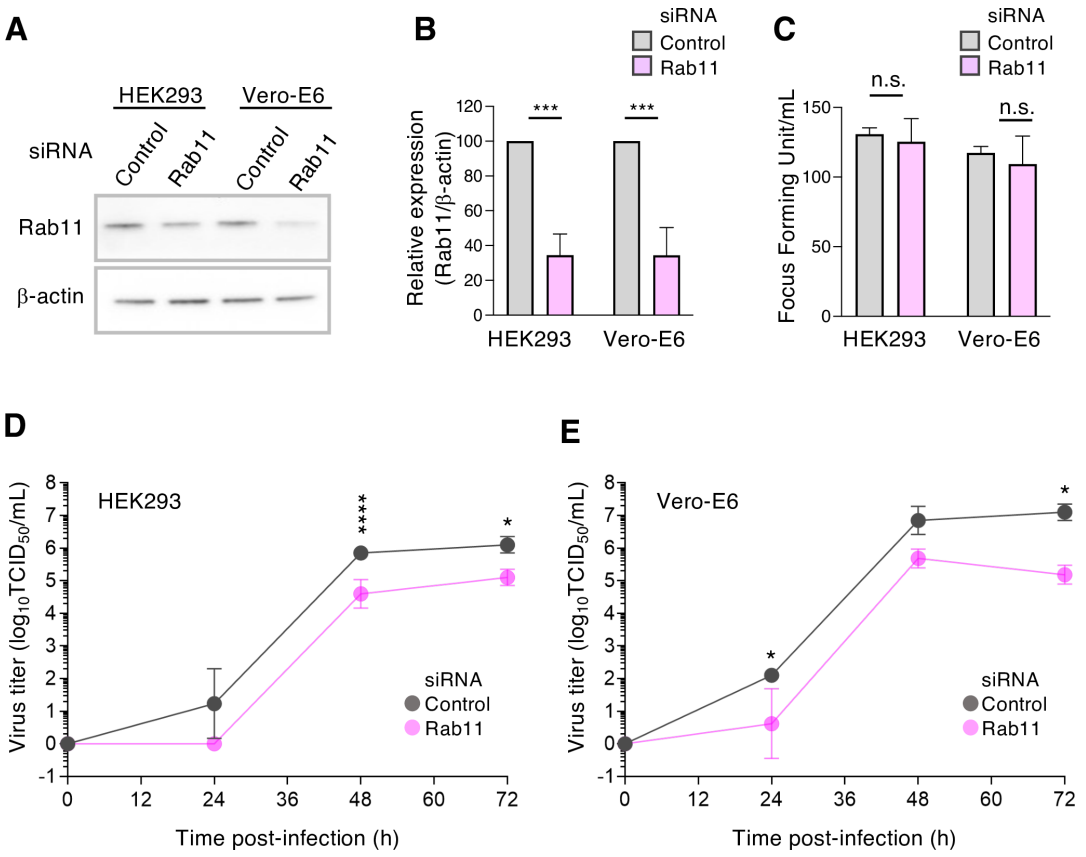

FIG 7 Effect of Rab11 downregulation on MARV particle production. (A) Downregulation of Rab11. HEK293 or Vero-E6 cells were transfected with siRNA against Rab11a and Rab11b. At 24 h.p.t., the expression of Rab11 in siRNA-treated cells was assessed by western blotting. The experiment was performed three times independently, and the representative blot is shown. (B) The intensity of corresponding bands to Rab11 was normalized with that of the β-actin band. The mean and SD are shown. (C) The effect of Rab11 knockdown on infection with MARV. siRNA-treated cells were inoculated with MARV at an MOI of 0.01 and subjected to the focus-forming assay. (D and E) The effect of Rab11 knockdown on the release of MARV production. Virus titers in the culture media collected at 0, 24, 48, and 72 h post-infection were analyzed by the $TCID_{50}$ assay using Vero-E6 cells. The experiment was performed three times independently, and the geometric mean ± SD are shown. n.s., not significant, $^{*}P < 0.05$; $^{***}P < 0.001$; $^{****}P < 0.0001$ versus respective control (Student's *t* test).

demonstrated that Rab11 downregulation interfered with the release of both VLP (Fig. 6) and infectious viral particles (Fig. 7).

The diverse functions mediated by Rab11 are regulated by interactions with Rab11 family interacting proteins (Rab11-FIPs) (58). Various FIP members are involved in the egress process to release RSV (42) and filamentous IAV virions (43) from the PM, suggesting that Rab11-associated effector proteins synergistically upregulate the scission process of filoviruses in addition to the ESCRT machinery. Negative effects of nocodazole treatment on the VLP formation may be derived from the reduction of traffic of Rab11-positive vesicles at the budding sites and subsequent scission process. Rab11 forms complexes with specific motor proteins via interactions with distinct adaptor proteins and promotes the bidirectional transport of recycling endosomes, which is mediated by the microtubule network and actin-filament-dependent transport (56). Rab11 has been suggested to form a ternary complex with the myosin Vb motor protein and FIP1 to tether Rab11-positive vesicles to actin filaments at the microtubule-actin junction and contribute to delivery to the PM (59). Rab11-FIP3 is responsible for the formation of a ternary complex with the cytoplasmic dynein motor protein and mediates vesicle transport from peripheral sorting endosomes to the centrally located endosomal recycling compartment through the microtubule minus-end transport system (60). In addition, Rab11-interacting protrudin facilitates the interaction between Rab11 and kinesin family member (KIF) 5a and subsequent microtubule plus-end directed vesicle

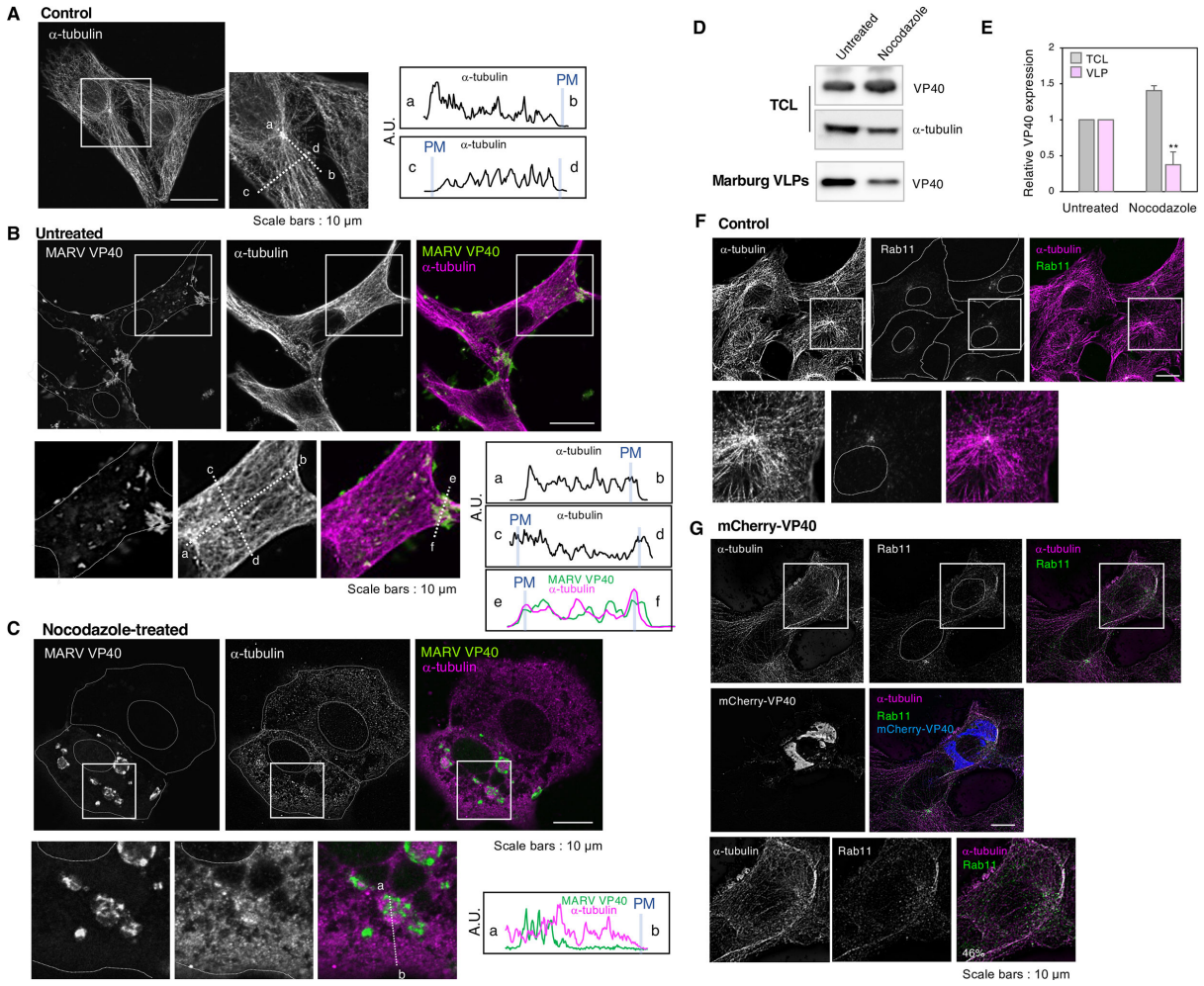

FIG 8 VP40 exploits the microtubule network for self and Rab11-positive vesicle trafficking for efficient VLP formation. (A–C) Effect of VP40 on the distribution of the microtubule network. Vero-E6 cells were transfected with the expression plasmids for MARV VP40. At 4 h.p.t., the cells were treated with DMSO (B) 1 μg/mL nocodazole (C) and further incubated for 20 h. As a control, the cells were transfected with a backbone plasmid (A). The subcellular distribution of VP40 and α-tubulin was analyzed using immunofluorescence staining. Ten cells in three fields were analyzed; the representative images are shown. The nuclei were counterstained with Hoechst 33342, and the dotted lines indicate their outlines. Cell peripheries were determined by phase contrast images and shown in lines. Insets show the box area. The plots indicate individual fluorescence intensities along each line. The location of the PM is shown in pale blue bars. A.U.; arbitrary unit. Arrows represent co-localized signals. Scale bars: 10 μm. (D and E) Effect of depolymerization of microtubule on VLP formation. HEK293T cells were transfected with MARV VP40. At 4 h.p.t., the cells were treated with 1 μg/mL nocodazole and further incubated for 44 h. As a control, the cells were treated with DMSO. The cells and culture medium were harvested. TCLs were subjected to western blotting with the antibodies against VP40 or α-tubulin (D). The intensity of the band's correspondence to VP40 was quantified and normalized with that of α-tubulin (E, gray). VLPs in the culture medium were purified by ultracentrifugation and subjected to western blotting with an antibody for VP40 (D). The intensity of the bands was quantified corresponding to VP40 (E, pink). The experiment was performed three times independently, and representative blots and the mean ± SD are shown. **, $P < 0.01$ versus respective control (Student's *t* test). (F and G) VP40-mediated dispersed distribution of Rab11 is dependent on the microtubule network. Vero-E6 cells were transfected with the expression plasmids for mCherry-fused MARV VP40 and VP40 at a ratio of 1:5. At 24 h.p.t., the cells were harvested, and the subcellular distribution of VP40, Rab11, and α-tubulin was analyzed using immunofluorescence staining. Ten cells in three fields were analyzed; the representative images are shown. The nuclei were counterstained with Hoechst 33342, and the dotted lines indicate their outlines. Cell peripheries were determined by phase contrast images and shown in dotted lines. Insets show the box area. Proportion of Rab11 co-localized with α-tubulin was measured using the IMARIS imaging software and shown in the image. Scale bars: 10 μm.

transport (61). Another plus-end-directed kinesin motor, KIF3, interacts directly with the FIP5 adaptor protein and regulates endocytic protein recycling at the perinuclear recycling endosome (62).

We further observed that VP40 partly associated with microtubules (Fig. 8B and 9A) and promoted the microtubule network distribution toward the cell periphery (Fig. 8B and G). Depolymerization of microtubules under treatment with nocodazole abrogated the cluster formation of VP40 at the cell periphery and VLP production (Fig. 8C through E). The interaction of VP40 with α-tubulin remained even after treatment with nocodazole (Fig. 9B). These data indicate that the intracellular transport of VP40 and VLP formation require microtubule network dynamics. Moreover, dispersed Rab11 signals partly co-localized with microtubules in cells expressing VP40 (Fig. 8G). These data suggest that VP40 interacts with microtubules and modulates their dynamics, leading to the trafficking of microtubule-associated Rab11-positive vesicles toward the PM.

A previous study demonstrated that EBOV VP40 directly associates with the microtubule network via its partially homologous sequence with the tubulin-binding motif of the host microtubule-associated protein 2 and induces tubulin polymerization (27). Ten amino acids in EBOV VP40 have been shown to be identical to the tubulin-binding motif of MAP2 consisting of 31 amino acids. MARV VP40 possesses three amino acids that are homologous to the motif in MAP2, suggesting that unknown mechanisms, independent of this motif, may be responsible for its interaction with microtubules.

In our previous study, two VP40 mutants, which were functionally defective in VLP formation due to failure of dimerization and further oligomerization, did not affect the intracellular distribution of Rab11 (49), suggesting that dimer formation of VP40 is important for Rab11-mediated EBOV particle production. MARV and EBOV VP40 share a 49% amino acid sequence homology. Crystal structure studies have shown that the N-terminal domains of both VP40s are similar in structure and contribute to dimer formation, which further assembles into a flexible filamentous matrix (63, 64). In contrast, the C-terminal domain of MARV VP40 is more loosely folded than that of EBOV VP40 and exhibits an extended, highly basic patch covering one side. Thus, further stoichiometric analyses are required to understand the mechanism by which MARV VP40 interacts with microtubules. Moreover, multiple host cytoskeletal factors, including actin (65–67) are responsible for the intracellular transport of VP40. Thus, these complexes of Rab11 effector proteins and various motor proteins likely mediate the traffic of VP40 that associates with cytoskeletal networks to the PM, which is responsible for virion formation and egress. Further characterization of the Rab11-associated effector proteins underlying this process is required to better understand the detailed molecular mechanisms by which Rab11 contributes to the intracellular trafficking of VP40 and the formation of filovirus particles.

Data in our previous and present studies showed that neither EBOV VP40 (49) nor MARV VP40 efficiently co-localize with endogenous Rab11 (Fig. 1) and GFP-wtRab11 (Fig. 4). A possible explanation for their inefficient co-localization is that VP40 is associated indirectly via the microtubule network with Rab11, which is expressed in the vesicles. Our study also demonstrated a lack of direct association between VP40 and GFP-Rab11 derivatives (Fig. 9C). This is because only a few Rab11-positive vesicles are associated with precipitated microtubule and/or the interaction may be disrupted by detergent treatment. Further investigation by use of live-cell imaging and/or the native immunoprecipitation in the context of an authentic MARV infection system can be applied to confirm their indirect association under the physiological condition.

The effect of the treatment of siRNA against Rab11 on the release of VLPs and viral particles was moderate (Fig. 6 and 7), which may be partly due to the incomplete knockdown of Rab11 molecules and/or the existence of a Rab11-independent mechanism responsible for viral particle formation. In addition, the lack of statistical significance for the reduction of progeny MARV by knockdown of Rab11 at certain time points after infection is also likely due to the variability derived from the cell-based titration assay. Nevertheless, the reduction of virus titer exhibited statistical significance in both cell types with the treatment of siRNA against Rab11 at 72 h.p.i., wherein MARV replication reaches a plateau in the same cell type (68, 69).

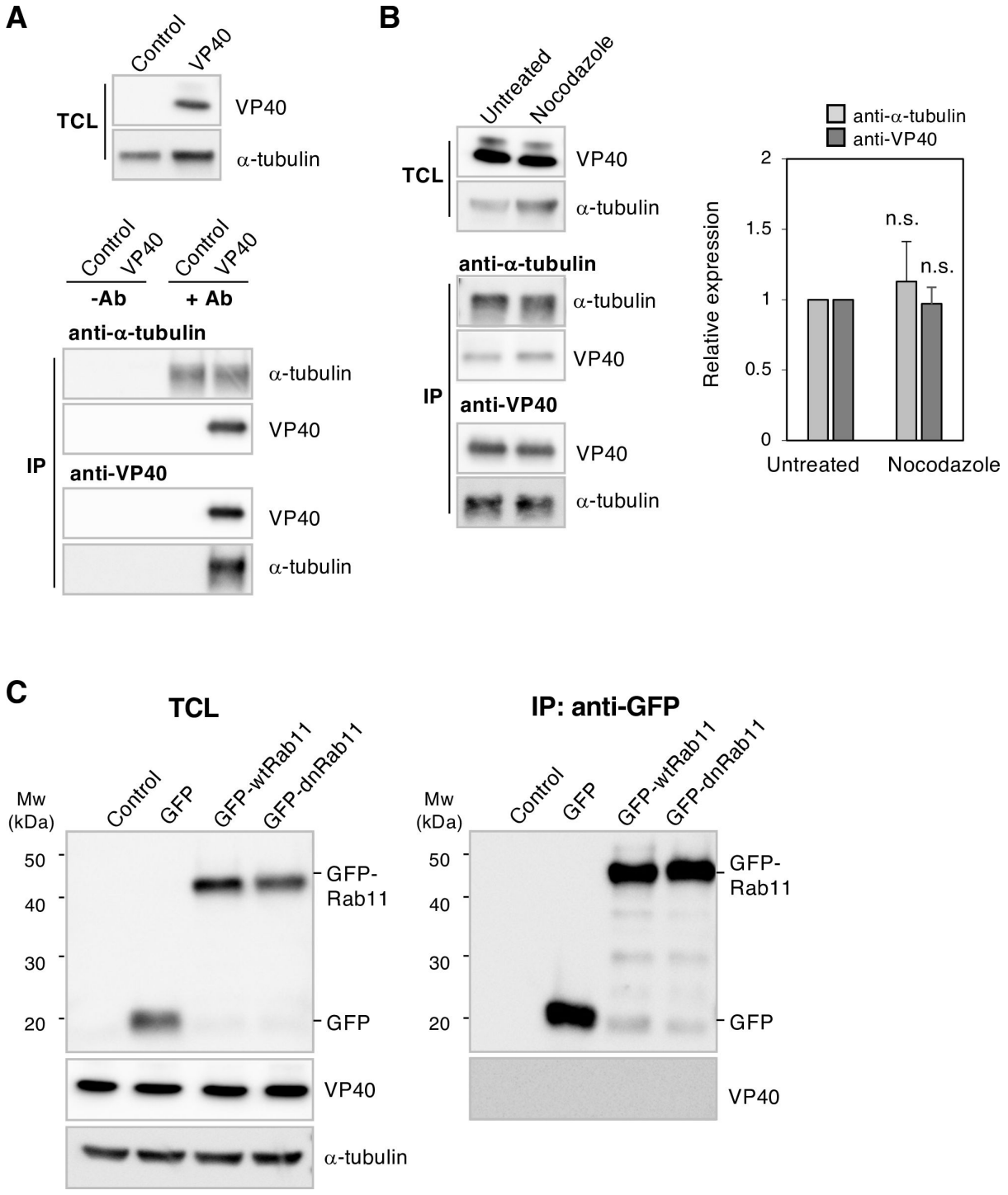

FIG 9 VP40 interacts with α-tubulin but not with Rab11. (A and B) Interaction of VP40 with α-tubulin. HEK293T cells were transfected with the expression plasmids for VP40. At 4 h.p.t., the cells were treated with 1 µg/mL nocodazole for 44 h. As a control, the cells were treated with DMSO. The cells were harvested and lysed with the tubulin-binding buffer. Lysate was incubated with polyclonal antibodies against α-tubulin or MARV VP40 and Protein G Sepharose (+Ab). As a control, lysate was incubated with Protein G Sepharose alone (−Ab). Immunoprecipitants were subjected to western blotting using anti-VP40 antibody. The intensity of the band's correspondence to co-precipitated VP40 or α-tubulin was quantified and normalized with that of α-tubulin or VP40, respectively. The experiment was performed three times independently, and representative blots (A) and the mean ± SD (B) are shown. n.s., not significant versus respective control (Student's *t* test). (C) Interaction of VP40 with Rab11. HEK293T cells were transfected with the expression plasmids for VP40 along with GFP, GFP-wtRab11, or GFP-dnRab11. At 48 h.p.t., the cells were harvested and lysed with RIPA buffer. Lysate was incubated with anti-GFP antibody-conjugated magnetic beads. Immunoprecipitants were subjected to western blotting using antibodies against VP40, GFP, or α-tubulin. The experiment was performed three times independently, and representative blots are shown.

Taken together, our study demonstrates that MARV exploits the microtubule-dependent Rab11-mediated PM-directed vesicle-trafficking pathway for the release of viral particles. This indicates that two distinct genera of the family *Filoviridae* commonly exploit the Rab11-dependent endocytic pathway for efficient viral particle formation, which may offer new potential targets for the development of pan-filovirus therapeutics.

MATERIALS AND METHODS

Cell culture

African green monkey kidney epithelial Vero-E6 cells and human embryonic kidney HEK293 cells (American Type Culture Collection) were grown in high-glucose Dulbecco's modified Eagle's medium (DMEM) (Wako Pure Chemical, Osaka, Japan) containing 10% fetal bovine serum (FBS) (Sigma-Aldrich, St. Louis, MO, USA), 100 U/mL penicillin, and 100 µg/mL streptomycin (Wako Pure Chemical). Cells were maintained at 37°C in 5% CO_2. Expi293F cells (kindly gifted by Dr. Kentaro Yoshii, Nagasaki University) were grown in Expi293 expression medium (Thermo Fisher Scientific, Waltham, MA, USA) and maintained at 37°C in 8% CO_2.

Plasmids

The pCAGGS-based expression plasmids of MARV subtype Lake Victoria, variant Angola VP40, NP, and GP were gifted by Dr. Ayato Takada (Hokkaido University). The pCAGGS-EBOV subtype Zaire, isolate Mayinga VP40 plasmid was gifted by Dr. Yoshihiro Kawaoka (National Center for Global Health and Medicine). The pEGFP-C3 plasmids encoding enhanced GFP-fused wild-type Rab11 (GFP-wtRab11) and the dominant-negative form of Rab11 (GFP-Rab11S25N) were kindly provided by Dr. Angela Wandinger-Ness (University of New Mexico) (30). The expression plasmids of mCherry-fused MARV VP40 were constructed by insertion of a PCR-amplified VP40 fragment into the mCherry-C1 plasmid.

Immunofluorescence staining

Vero-E6 cells grown on coverslips were transfected with the expression plasmids for filovirus VP40, NP, or GP or the expression plasmid encoding GFP-fused Rab11 derivatives using TransIT-X2 (Mirus Bio, Madison, WI, USA). At 24 or 48 h.p.t., the cells were fixed with 4% paraformaldehyde in phosphate-buffered saline (PBS) for 10 min at room temperature, permeabilized with PBS containing 0.05% Triton X-100 for 10 min at room temperature, and blocked in PBS containing 2% bovine serum albumin for 20 min at room temperature. The cells were then incubated with a rabbit polyclonal antibody against Rab11 (Abcam, Cambridge, UK; 1:200 dilution) and/or a mouse monoclonal antibody against MARV VP40 (clone 1-17-1; 1:1,000 dilution; gifted by Dr. Ayato Takada), NP (clone 6H9; 1:1,000 dilution; gifted by Dr. Ayato Takada), GP (clone 127-8; 1:1,000 dilution; gifted by Dr. Ayato Takada), EBOV VP40 (clone 6; 1:1,000 dilution; gifted by Dr. Yoshihiro Kawaoka) for 1 h at room temperature. The cells were washed with PBS and incubated with Alexa Fluor 488-, 594-, or 647-labeled secondary antibodies (Thermo Fisher Scientific, 1:2,000 dilution) for 1 h at room temperature. After washing, nuclei were counterstained with Hoechst 33342 (Cell Signaling Technology, Trask Lane, MA, USA). To determine the effect of GFP-wtRab11 or -dnRab11 on the distribution of MARV VP40, we transfected Vero-E6 cells with expression plasmids encoding GFP-wtRab11 or -dnRab11 along with that for MARV VP40. At 48 h.p.t., the cells were harvested and subjected to immunofluorescence staining with the mouse monoclonal antibody for MARV VP40 (clone 1-17-1; 1:1,000). To characterize the effect of MARV VP40 on the distribution of microtubules and Rab11, the cells were transfected with the expression plasmids for mCherry-fused MARV VP40 and MARV VP40 in the ratio of 1:5. At 24 h.p.t., the cells were harvested and incubated with the rabbit antibody for Rab11 (Abcam; 1:200 dilution) and the mouse monoclonal antibody for α-tubulin (clone DM1A, Abcam; 1:200). To analyze the effect of VP40 on the microtubule network, the cells were transfected with the

expression plasmid for MARV VP40. At 4 h.p.t., the cells were treated with or without 1 µg/mL nocodazole (Sigma-Aldrich) for 20 h. The cells were harvested and subjected to immunofluorescence staining with a mouse monoclonal antibody for MARV VP40 (clone 1-17-1; 1:1000) and a rabbit polyclonal antibody for α-tubulin (Medical & Biological Laboratories, Tokyo, Japan; 1:1,000). Images were taken using a confocal laser scanning microscope with oil emersion objective lens at magnification 60× (Fluoview FV3000, Evident Scientific, Tokyo, Japan) using FV31S-SW software (Evident Scientific).

Image analysis

For quantification of the intracellular distribution of Rab11-positive vesicles, images for more than 10 cells in three to five fields were acquired with a z-stack of approximately 20 slices at 0.2 µm intervals. Z-stack images were reconstructed with imaging software (IMARIS; OXFORD Instruments, Oxfordshire, UK), and the surface area (μm^2) of the cell and the nucleus of the examined cells were analyzed using the ImarisCell module. Distance (µm) between the Rab11-positive signals and the closest nucleus and the volumes in single cells were analyzed using the ImarisCell module. The cellSens (Evident Scientific) was used to calculate the maximal fluorescence intensity of the channels to determine the distribution of the individual fluorescence signals. To determine the localization of Rab11 and microtubules, z-stack images were further processed by deconvolution. Images are shown by maximal intensity projection. For intensity-based co-localization analysis of Rab11 and α-tubulin, images for more than 10 cells in three to five fields were acquired with a z-stack of approximately 20 slices at 0.2 µm intervals. Z-stack images were reconstructed and analyzed using the ImarisCo-loc module.

Characterization of Rab11 incorporation in MARV VLPs

Marburg VLPs were prepared following the procedures for preparing Ebola VLPs (51, 70). Equal amounts of the pCAGGS expression plasmids for MARV VP40, GP, and NP were transfected into Expi293F cells using ExpiFectamine (Thermo Fisher Scientific) according to the manufacturer's instructions. At 48 h.p.t., the culture supernatants were harvested and centrifuged at 440 × *g* for 5 min and then at 2,380 × *g* for 15 min to remove detached cells and cell debris, respectively. The VLPs were precipitated through a 30% sucrose cushion by ultracentrifugation at 14,860 × *g* for 1 h at 4°C with an SW32Ti rotor (Beckman, Fullerton, CA, USA). The precipitated VLPs were resuspended in TNE buffer [10 mM Tris-HCl (pH 8.0), 100 mM NaCl, and 1 mM EDTA] and fractionated using a 30%–60% sucrose gradient in TNE buffer at 89,527 × *g* for 2.5 h at 4°C with the SW32Ti rotor. The expression of MARV VP40 in each fraction was determined by western blotting using a mouse anti-MARV VP40 monoclonal antibody (clone 1-17-1; 1:1,000 dilution). The fractions corresponding to VLPs were collected, and VLPs were concentrated by ultracentrifugation at 14,860 × *g* for 1 h at 4°C with the SW32Ti rotor. The amount of protein in the VLP suspension was determined using the Bradford protein assay kit (Bio-Rad Laboratories, CA, USA). The morphology of the purified VLPs was confirmed using transmission electron microscopy. The incorporation of Rab11 into Marburg VLPs was characterized by a western blotting-based protease protection assay (49). About 2 µg VLPs was treated with or without 0.05% Triton X-100 for 10 min, then in the presence or absence of 0.1 mg/mL trypsin (Sigma-Aldrich) for another 10 min at room temperature. VLPs were then incubated in Laemmli sample buffer for 5 min at 95°C, followed by western blotting using the mouse monoclonal antibodies against MARV VP40 (clone 1-17-1; 1:1,000 dilution) and Rab11 (BD Biosciences, Franklin Lakes, NJ, USA; 1:1,000 dilution). Band intensity was quantified using CSAnalyzer4 software Ver. 4 (ATTO Corporation, Tokyo, Japan).

Negative-staining electron microscopy

VLPs were fixed with 2.5% glutaraldehyde (Electron Microscopy Sciences, Hatfield, PA, USA) in 0.1 M cacodylate buffer (pH 7.4) (Nacalai Tesque Inc., Kyoto, Japan) overnight at

4°C. Each sample was loaded onto a 200-mesh copper grid with a carbon-coated plastic film (Nisshin EM, Tokyo, Japan) immediately following glow discharge and negatively stained with uranyl acetate solution (1%, wt/vol) for 15 s. The morphology of each sample was observed using a JEM-1400Flash microscope (JEOL, Tokyo, Japan) with an acceleration voltage of 80 kV.

Effect of downregulation of Rab11 or microtubule modulators on Marburg VLPs production

To elucidate the effect of the downregulation of Rab11, siRNAs targeting human Rab11a and Rab11b (Thermo Fisher Scientific) were transfected into HEK293 cells using TransIT-X2. As a control, a siRNA encoding a sequence that does not target any known gene (Thermo Fisher Scientific) was transfected. At 72 h.p.t, Rab11 downregulation was confirmed by western blotting using the mouse monoclonal antibody for Rab11 (BD Biosciences; 1:1,000 dilution) and a rabbit polyclonal antibody for α-tubulin (Medical & Biological Laboratories; 1:1,000 dilution). The siRNA-treated cells were transfected with expression plasmids encoding MARV VP40, NP, and GP using TransIT-X2. At 48 h.p.t., the culture supernatant was harvested and centrifuged at 440 × *g* for 5 min and then at 2,380 × *g* for 15 min. VLPs were precipitated through a 20% sucrose cushion by ultracentrifugation at 14,860 × *g* for 1 h at 4°C with an SW32Ti rotor. The precipitated VLPs were suspended in the TNE buffer. Expression of MARV proteins in the total cell lysates (TCLs) and the purified VLPs was determined by western blotting using mouse monoclonal antibodies against MARV VP40 (clone 1-17-1; 1:1,000 dilution), NP (clone FS0609; 1:1,000 dilution, gifted by Dr. Ayato Takada), GP (clone 127-8; 1:1,000 dilution, gifted by Dr. Ayato Takada), and a rabbit polyclonal antibody for α-tubulin (Medical & Biological Laboratories; 1:1,000 dilution). Band intensity was quantified using the CSAnalyzer4 software. To examine the effect of microtubule modulators on VLP formation, HEK293T cells were transfected with the expression plasmids for MARV VP40 using TransIT-X2 (Mirus). At 4 h.p.t., the cells were treated with or without 1 µg/mL nocodazole (Sigma-Aldrich) for 44 h. As a control, the cells were treated with dimethyl sulfoxide (DMSO) (Nacalai Tesque Inc.). Expression of VP40 in the TCLs and production of harvested Marburg VLPs in the supernatant were determined as described above.

Effect of Rab11 downregulation on the release of authentic MARV

siRNAs targeting human Rab11a and Rab11b (Thermo Fisher Scientific) or control siRNAs were transfected into HEK293 or Vero-E6 cells using Transit-TKO (Mirus). At 24 h.p.t., Rab11 downregulation was confirmed by western blotting using a mouse monoclonal antibody for Rab11 (BD Biosciences; 1:1,000 dilution) and a mouse monoclonal antibody for β-actin (Sigma-Aldrich, clone AC-15; 1:1,000 dilution). To determine the effect of Rab11 knockdown on infection with MARV-Angola (GenBank accession: KY047763), we infected siRNA-transfected cells with MARV at an MOI of 0.01 and incubated them for 1 h at 37°C. The cells were washed three times with DMEM and covered with Eagle's minimal essential medium containing 2% FBS (Thermo Fisher Scientific) and 1.2% carboxymethyl cellulose (Sigma-Aldrich). After incubation for 2 days, the cells were fixed with 10% phosphate-buffered formalin overnight at 4°C, and the effect of Rab11 knockdown on viral infection was determined using a focus-forming assay (FFA). MARV-infected cells were observed by immunofluorescence staining with a mouse anti-MARV VP40 antibody (clone 1-17-1; 1:400 dilution). The MARV titers were quantified by measuring the number of fluorescent foci using a ZOE fluorescent cell imager (Bio-Rad). To analyze the effect of Rab11 downregulation on the release of progeny MARV, we inoculated siRNA-transfected cells with MARV at an MOI of 0.01 24 h after siRNA treatment and further incubated them for 1 h at 37°C. The cells were washed three times with DMEM and cultured in DMEM containing 2% FBS. Supernatants were collected at 0, 24, 48, and 72 h post-infection, and the titer of MARV in the supernatant was measured using a median tissue culture infectious dose ($TCID_{50}$) assay on Vero-E6 cells.

All infectious work with MARV was performed in the biosafety level-4 laboratory at the Integrated Research Facility at the Rocky Mountain Laboratories, Division of Intramural Research, National Institute of Allergy and Infectious Diseases, National Institutes of Health, Hamilton, Montana, USA. All experiments followed standard operating procedures which were approved by the Institutional Biosafety Committee.

Immunoprecipitation

To determine the association of MARV VP40 with α-tubulin, HEK293T cells were transfected with the expression plasmid for MARV VP40 using TransIT-X2. The backbone plasmid was transfected as a control. At 48 h.p.t., the cells were lysed with the tubulin-binding buffer [80 mM HEPES (pH 7.6), 10% Triton X-100, 1 mM $MgCl_2$, and 1 mM EGTA] containing 1 mM Phenylmethylsulfonyl fluoride (PMSF), 2 µg/µL Leupeptin, 2 µg/µL Pepstatin A, and 2 µg/µL Aprotinin for 1 h at room temperature. After ultracentrifugation at 12,000 × *g* for 10 min, the supernatants were incubated with 1 µg/mL rabbit polyclonal antibody against α-tubulin (Medical & Biological Laboratories) or with a 1 µg/mL rabbit polyclonal antibody for VP40 (Integrated BioTherapeutics, Rockville, MD, USA) for 1 h at room temperature. Protein G Sepharose (Cytiva, Marlborough, MA, USA) was added to the supernatants and incubated for 1 h at room temperature. As a control, cell lysates were incubated with Protein G Sepharose alone. Sepharose was washed three times in the same buffer and immunoprecipitants were subjected to western blotting using a mouse monoclonal antibody against MARV VP40 (clone 1-17-1; 1:1,000 dilution) and α-tubulin (Abcam; 1:1,000 dilution).

To characterize the interaction of MARV VP40 with Rab11, HEK293T cells were transfected with the expression plasmids for MARV VP40, and GFP or GFP-fused Rab11 derivatives using TransIT-X2. As a control, the backbone plasmid was co-transfected. At 48 h.p.t., the cells were lysed with radioimmunoprecipitation assay (RIPA) buffer (Nacalai Tesque Inc.) containing 1 mM PMSF, 2 µg/µL Leupeptin, 2 µg/µL Pepstatin A, and 2 µg/µL Aprotinin for 1 h at 4°C. After ultracentrifugation at 12,000 × *g* for 10 min, the supernatants were incubated with the anti-GFP antibody-conjugated magnetic beads (Medical & Biological Laboratories) for 1 h at 4°C. Immunoprecipitants were subjected to western blotting using the mouse monoclonal antibodies against MARV VP40 (clone 1-17-1; 1:1,000 dilution) and the rabbit polyclonal antibodies for GFP (Medical & Biological Laboratories; 1:1,000 dilution) and α-tubulin (Medical & Biological Laboratories; 1:1,000 dilution).

Statistical analysis

For image analysis, images of more than 10 cells in 3–10 fields were acquired per sample, and the analyzed data were subjected to Student's *t* test for statistical analysis. For western blot analysis, FFA, and $TCID_{50}$ assay, experiments were independently performed more than three times and subjected to Student's *t* test or one-way ANOVA for statistical analysis.

ACKNOWLEDGMENTS

The authors thank Dr. Ayato Takada (Hokkaido University) for providing the expression plasmids for MARV VP40, NP, and GP, and the antibodies for MARV VP40, NP, and GP. Dr. Yoshihiro Kawaoka (National Center for Global Health and Medicine) for providing the expression plasmid for EBOV VP40 and antibody for EBOV VP40. The authors thank Dr. Angela Wandinger-Ness (University of New Mexico) and Dr. Kentaro Yoshii (Nagasaki University) for providing the pEGFP-C3 plasmids encoding GFP-fused Rab11 derivatives and Expi293F cells, respcetively. The authors also thank Ms. Hazuki Sakumoto (Nagasaki University) and Ms. Kayoko Sasabuchi (Nagasaki University) for technical assistances. The authors thank Dr. Heinz Feldmann for the critical review of the manuscript and constructive comments.

This work was supported by grants from the Japan Society for the Promotion of Science (21K20762 and 23790493), Japan Agency for Medical Research and Development (21461223, JP22fm0208101, and JP23jf0126002), Japan Science and Technology Agency (01-117), Daiichi Sankyo Foundation of Life Science, Hayashi Memorial Foundation for Female Natural Scientists, Mochida Memorial Foundation for Medical and Pharmaceutical Research, Takeda Science Foundation, Chugai Foundation for Innovative Drug Discovery Science, Suhara Memorial Foundation, and the Akiyama Life Science Foundation, Joint Usage/Research Center programs from the Hokkaido University Research Center for Zoonosis Control, Institute of Medical Science, University of Tokyo, Institute for Frontier Life and Medical Sciences, Kyoto University, and Tropical Disease, Institute of Tropical Medicine (NEKKEN), Nagasaki University. This work was in part funded by Intramural Research Program, NIAID, NIH. The authors would also like to thank Editage for English language editing of the manuscript.

AUTHOR AFFILIATIONS

[1]National Research Center for the Control and Prevention of Infectious Diseases, Nagasaki University, Nagasaki, Japan
[2]Central Laboratory, Institute of Tropical Medicine (NEKKEN), Nagasaki University, Nagasaki, Japan
[3]Laboratory of Virology, Division of Intramural Research, National Institute of Allergy and Infectious Diseases, National Institutes of Health, Hamilton, Montana, USA

AUTHOR ORCIDs

Wakako Furuyama http://orcid.org/0000-0001-7163-6960
Miako Sakaguchi http://orcid.org/0000-0001-5105-3100
Andrea Marzi http://orcid.org/0000-0003-0186-9587
Asuka Nanbo http://orcid.org/0000-0001-8764-1350

FUNDING

Funder	Grant(s)	Author(s)
MEXT | Japan Society for the Promotion of Science (JSPS)	23790493, 21K20762	Wakako Furuyama Asuka Nanbo
Japan Agency for Medical Research and Development (AMED)	JP22fm0208101, 21461223, JP23jf0126002	Asuka Nanbo
MEXT | Japan Science and Technology Agency (JST)	01-117	Asuka Nanbo
Takeda Medical Research Foundation		Asuka Nanbo
Daiichi Sankyo Foundation of Life Science		Asuka Nanbo
Hayashi Memorial Foundation for Female Natural Scientists		Asuka Nanbo
Mochida Memorial Foundation for Medical and Pharmaceutical Research (公益財団法人 持田記念医学薬学振興財団)		Asuka Nanbo
Chugai Foundation for Innovative Drug Discovery Science		Asuka Nanbo
Suhara Memorial Foundation		Asuka Nanbo
Akiyama Life Science Foundation		Asuka Nanbo
Daiichi Sankyo Foundation of Life Science		Asuka Nanbo
HHS | NIH | NIAID | Division of Intramural Research (DIR, NIAID)		Andrea Marzi

AUTHOR CONTRIBUTIONS

Wakako Furuyama, Formal analysis, Funding acquisition, Methodology, Validation, Writing – original draft, Writing – review and editing | Kento Yamada, Data curation, Investigation, Validation, Visualization, Writing – original draft, Writing – review and editing | Miako Sakaguchi, Investigation, Methodology, Resources, Validation, Visualization, Writing – original draft, Writing – review and editing | Andrea Marzi, Data curation, Resources, Validation, Writing – original draft, Writing – review and editing | Asuka Nanbo, Conceptualization, Data curation, Formal analysis, Funding acquisition, Investigation, Methodology, Project administration, Resources, Supervision, Validation, Visualization, Writing – original draft, Writing – review and editing

ETHICS APPROVAL

Institutional review board statement: All infectious work with MARV was performed in the BSL-4 laboratory at the Integrated Research Facility at the Rocky Mountain Laboratories, Division of Intramural Research, National Institute of Allergy and Infectious Diseases, National Institutes of Health, Hamilton, Montana, USA. All experiments followed standard operating procedures which were approved by the Institutional Biosafety Committee.

REFERENCES

1. World Health Organization. 2021. Marburg virus disease. Available from: https://www.who.int/news-room/fact-sheets/detail/marburg-virus-disease
2. Hoenen T, Groseth A, Feldmann H. 2019. Therapeutic strategies to target the Ebola virus life cycle. Nat Rev Microbiol 17:593–606. https://doi.org/10.1038/s41579-019-0233-2
3. Jacob ST, Crozier I, Fischer WA, Hewlett A, Kraft CS, Vega M-A de L, Soka MJ, Wahl V, Griffiths A, Bollinger L, Kuhn JH. 2020. Ebola virus disease. Nat Rev Dis Primers 6:13. https://doi.org/10.1038/s41572-020-0147-3
4. Cross RW, Longini IM, Becker S, Bok K, Boucher D, Carroll MW, Díaz JV, Dowling WE, Draghia-Akli R, Duworko JT, et al. 2022. An introduction to the Marburg virus vaccine consortium, MARVAC. PLoS Pathog 18:e1010805. https://doi.org/10.1371/journal.ppat.1010805
5. Feldmann H, Sanchez A, Geisbert T. 2013. Filoviridae: Marburg and Ebola viruses. In Knipe M, Howley PM (ed), Fields virology, 6th ed. Lippincott Williams & Wilkins, Philadelphia, PA.
6. Noda T, Sagara H, Suzuki E, Takada A, Kida H, Kawaoka Y. 2002. Ebola virus VP40 drives the formation of virus-like filamentous particles along with GP. J Virol 76:4855–4865. https://doi.org/10.1128/JVI.76.10.4855-4865.2002
7. Timmins J, Scianimanico S, Schoehn G, Weissenhorn W. 2001. Vesicular release of Ebola virus matrix protein VP40. Virology 283:1–6. https://doi.org/10.1006/viro.2001.0860
8. Jasenosky LD, Neumann G, Lukashevich I, Kawaoka Y. 2001. Ebola virus VP40-induced particle formation and association with the lipid bilayer. J Virol 75:5205–5214. https://doi.org/10.1128/JVI.75.11.5205-5214.2001
9. Harty RN, Brown ME, Wang G, Huibregtse J, Hayes FP. 2000. A PPxY motif within the VP40 protein of Ebola virus interacts physically and functionally with a ubiquitin ligase: implications for filovirus budding. Proc Natl Acad Sci U S A 97:13871–13876. https://doi.org/10.1073/pnas.250277297
10. Makino A, Yamayoshi S, Shinya K, Noda T, Kawaoka Y. 2011. Identification of amino acids in Marburg virus VP40 that are important for virus-like particle budding. J Infect Dis 204:S871–S877. https://doi.org/10.1093/infdis/jir309
11. Kolesnikova L, Berghöfer B, Bamberg S, Becker S. 2004. Multivesicular bodies as a platform for formation of the Marburg virus envelope. J Virol 78:12277–12287. https://doi.org/10.1128/JVI.78.22.12277-12287.2004
12. Kolesnikova L, Bamberg S, Berghöfer B, Becker S. 2004. The matrix protein of Marburg virus is transported to the plasma membrane along cellular membranes: exploiting the retrograde late endosomal pathway. J Virol 78:2382–2393. https://doi.org/10.1128/JVI.78.5.2382-2393.2004
13. Shepley-McTaggart A, Fan H, Sudol M, Harty RN. 2020. Viruses go modular. J Biol Chem 295:4604–4616. https://doi.org/10.1074/jbc.REV119.012414
14. Yasuda J, Nakao M, Kawaoka Y, Shida H. 2003. Nedd4 regulates egress of Ebola virus-like particles from host cells. J Virol 77:9987–9992. https://doi.org/10.1128/JVI.77.18.9987-9992.2003
15. Timmins J, Schoehn G, Ricard-Blum S, Scianimanico S, Vernet T, Ruigrok RWH, Weissenhorn W. 2003. Ebola virus matrix protein VP40 interaction with human cellular factors Tsg101 and Nedd4. J Mol Biol 326:493–502. https://doi.org/10.1016/S0022-2836(02)01406-7
16. Han Z, Sagum CA, Bedford MT, Sidhu SS, Sudol M, Harty RN. 2016. ITCH E3 ubiquitin ligase interacts with Ebola virus VP40 to regulate budding. J Virol 90:9163–9171. https://doi.org/10.1128/JVI.01078-16
17. Han Z, Sagum CA, Takizawa F, Ruthel G, Berry CT, Kong J, Sunyer JO, Freedman BD, Bedford MT, Sidhu SS, Sudol M, Harty RN. 2017. Ubiquitin ligase WWP1 interacts with Ebola virus VP40 to regulate egress. J Virol 91. https://doi.org/10.1128/JVI.00812-17
18. Licata JM, Simpson-Holley M, Wright NT, Han Z, Paragas J, Harty RN. 2003. Overlapping motifs (PTAP and PPEY) within the Ebola virus VP40 protein function independently as late budding domains: involvement of host proteins TSG101 and VPS-4. J Virol 77:1812–1819. https://doi.org/10.1128/JVI.77.3.1812-1819.2003
19. Liang J, Djurkovic MA, Shtanko O, Harty RN. 2023. Chaperone-assisted selective autophagy targets filovirus VP40 as a client and restricts egress of virus particles. Proc Natl Acad Sci U S A 120:e2210690120. https://doi.org/10.1073/pnas.2210690120
20. Liang J, Sagum CA, Bedford MT, Sidhu SS, Sudol M, Han Z, Harty RN. 2017. Chaperone-mediated autophagy protein BAG3 negatively regulates Ebola and Marburg VP40-mediated egress. PLoS Pathog 13:e1006132. https://doi.org/10.1371/journal.ppat.1006132
21. Han Z, Ruthel G, Dash S, Berry CT, Freedman BD, Harty RN, Shtanko O. 2020. Angiomotin regulates budding and spread of Ebola virus. J Biol Chem 295:8596–8601. https://doi.org/10.1074/jbc.AC120.013171
22. Han Z, Dash S, Sagum CA, Ruthel G, Jaladanki CK, Berry CT, Schwoerer MP, Harty NM, Freedman BD, Bedford MT, Fan H, Sidhu SS, Sudol M, Shtanko O, Harty RN. 2020. Modular mimicry and engagement of the Hippo pathway by Marburg virus VP40: implications for filovirus biology and budding. PLoS Pathog 16:e1008231. https://doi.org/10.1371/journal.ppat.1008231
23. Liang J, Ruthel G, Freedman BD, Harty RN. 2022. WWOX-mediated degradation of AMOTp130 negatively affects egress of filovirus VP40 virus-like particles. J Virol 96:e0202621. https://doi.org/10.1128/jvi.02026-21
24. Liang J, Ruthel G, Sagum CA, Bedford MT, Sidhu SS, Sudol M, Jaladanki CK, Fan H, Freedman BD, Harty RN. 2021. Angiomotin counteracts the

negative regulatory effect of host WWOX on viral PPxY-mediated egress. J Virol 95. https://doi.org/10.1128/JVI.00121-21
25. Lu J, Qu Y, Liu Y, Jambusaria R, Han Z, Ruthel G, Freedman BD, Harty RN. 2013. Host IQGAP1 and Ebola virus VP40 interactions facilitate virus-like particle egress. J Virol 87:7777–7780. https://doi.org/10.1128/JVI.00470-13
26. Yamayoshi S, Noda T, Ebihara H, Goto H, Morikawa Y, Lukashevich IS, Neumann G, Feldmann H, Kawaoka Y. 2008. Ebola virus matrix protein VP40 uses the COPII transport system for its intracellular transport. Cell Host Microbe 3:168–177. https://doi.org/10.1016/j.chom.2008.02.001
27. Ruthel G, Demmin GL, Kallstrom G, Javid MP, Badie SS, Will AB, Nelle T, Schokman R, Nguyen TL, Carra JH, Bavari S, Aman MJ. 2005. Association of Ebola virus matrix protein VP40 with microtubules. J Virol 79:4709–4719. https://doi.org/10.1128/JVI.79.8.4709-4719.2005
28. Pereira LE, Clark J, Grznarova P, Wen X, LaCasse R, Ruml T, Spearman P, Hunter E. 2014. Direct evidence for intracellular anterograde co-transport of M-PMV Gag and Env on microtubules. Virology 449:109–119. https://doi.org/10.1016/j.virol.2013.11.006
29. Wilcke M, Johannes L, Galli T, Mayau V, Goud B, Salamero J. 2000. Rab11 regulates the compartmentalization of early endosomes required for efficient transport from early endosomes to the trans-golgi network. J Cell Biol 151:1207–1220. https://doi.org/10.1083/jcb.151.6.1207
30. Chen W, Feng Y, Chen D, Wandinger-Ness A. 1998. Rab11 is required for trans-golgi network-to-plasma membrane transport and a preferential target for GDP dissociation inhibitor. MBoC 9:3241–3257. https://doi.org/10.1091/mbc.9.11.3241
31. Ullrich O, Reinsch S, Urbé S, Zerial M, Parton RG. 1996. Rab11 regulates recycling through the pericentriolar recycling endosome. J Cell Biol 135:913–924. https://doi.org/10.1083/jcb.135.4.913
32. Urbé S, Huber LA, Zerial M, Tooze SA, Parton RG. 1993. Rab11, a small GTPase associated with both constitutive and regulated secretory pathways in PC12 cells. FEBS Lett 334:175–182. https://doi.org/10.1016/0014-5793(93)81707-7
33. Takahashi S, Kubo K, Waguri S, Yabashi A, Shin HW, Katoh Y, Nakayama K. 2012. Rab11 regulates exocytosis of recycling vesicles at the plasma membrane. J Cell Sci 125:4049–4057. https://doi.org/10.1242/jcs.102913
34. Yoon SO, Shin S, Mercurio AM. 2005. Hypoxia stimulates carcinoma invasion by stabilizing microtubules and promoting the Rab11 trafficking of the α6β4 integrin. Cancer Res 65:2761–2769. https://doi.org/10.1158/0008-5472.CAN-04-4122
35. Westlake CJ, Baye LM, Nachury MV, Wright KJ, Ervin KE, Phu L, Chalouni C, Beck JS, Kirkpatrick DS, Slusarski DC, Sheffield VC, Scheller RH, Jackson PK. 2011. Primary cilia membrane assembly is initiated by Rab11 and transport protein particle II (TRAPPII) complex-dependent trafficking of Rabin8 to the centrosome. Proc Natl Acad Sci U S A 108:2759–2764. https://doi.org/10.1073/pnas.1018823108
36. Cox D, Lee DJ, Dale BM, Calafat J, Greenberg S. 2000. A Rab11-containing rapidly recycling compartment in macrophages that promotes phagocytosis. Proc Natl Acad Sci U S A 97:680–685. https://doi.org/10.1073/pnas.97.2.680
37. Chambers R, Takimoto T. 2010. Trafficking of Sendai virus nucleocapsids is mediated by intracellular vesicles. PLoS ONE 5:e10994. https://doi.org/10.1371/journal.pone.0010994
38. Stone R, Hayashi T, Bajimaya S, Hodges E, Takimoto T. 2016. Critical role of Rab11a-mediated recycling endosomes in the assembly of type I parainfluenza viruses. Virology 487:11–18. https://doi.org/10.1016/j.virol.2015.10.008
39. Varthakavi V, Smith RM, Martin KL, Derdowski A, Lapierre LA, Goldenring JR, Spearman P. 2006. The pericentriolar recycling endosome plays a key role in Vpu-mediated enhancement of HIV-1 particle release. Traffic 7:298–307. https://doi.org/10.1111/j.1600-0854.2005.00380.x
40. Diederich S, Sauerhering L, Weis M, Altmeppen H, Schaschke N, Reinheckel T, Erbar S, Maisner A. 2012. Activation of the Nipah virus fusion protein in MDCK cells is mediated by cathepsin B within the endosome-recycling compartment. J Virol 86:3736–3745. https://doi.org/10.1128/JVI.06628-11
41. Brock SC, Goldenring JR, Crowe JE. 2003. Apical recycling systems regulate directional budding of respiratory syncytial virus from polarized epithelial cells. Proc Natl Acad Sci U S A 100:15143–15148. https://doi.org/10.1073/pnas.2434327100
42. Utley TJ, Ducharme NA, Varthakavi V, Shepherd BE, Santangelo PJ, Lindquist ME, Goldenring JR, Crowe JE. 2008. Respiratory syncytial virus uses a Vps4-independent budding mechanism controlled by Rab11-FIP2. Proc Natl Acad Sci U S A 105:10209–10214. https://doi.org/10.1073/pnas.0712144105
43. Bruce EA, Digard P, Stuart AD. 2010. The Rab11 pathway is required for influenza A virus budding and filament formation. J Virol 84:5848–5859. https://doi.org/10.1128/JVI.00307-10
44. Sfakianos JN, LaCasse RA, Hunter E. 2003. The M-PMV cytoplasmic targeting-retention signal directs nascent Gag polypeptides to a pericentriolar region of the cell. Traffic 4:660–670. https://doi.org/10.1034/j.1600-0854.2003.00125.x
45. Arnaud F, Murcia PR, Palmarini M. 2007. Mechanisms of late restriction induced by an endogenous retrovirus. J Virol 81:11441–11451. https://doi.org/10.1128/JVI.01214-07
46. Coller KE, Heaton NS, Berger KL, Cooper JD, Saunders JL, Randall G. 2012. Molecular determinants and dynamics of hepatitis C virus secretion. PLoS Pathog 8:e1002466. https://doi.org/10.1371/journal.ppat.1002466
47. Kolesnikova L, Bugany H, Klenk HD, Becker S. 2002. VP40, the matrix protein of Marburg virus, is associated with membranes of the late endosomal compartment. J Virol 76:1825–1838. https://doi.org/10.1128/JVI.76.4.1825-1838.2002
48. Spurgers KB, Alefantis T, Peyser BD, Ruthel GT, Bergeron AA, Costantino JA, Enterlein S, Kota KP, Boltz RCD, Aman MJ, DelVecchio VG, Bavari S. 2010. Identification of essential filovirion-associated host factors by serial proteomic analysis and RNAi screen. Mol Cell Proteomics 9:2690–2703. https://doi.org/10.1074/mcp.M110.003418
49. Nanbo A, Ohba Y. 2018. Budding of Ebola virus particles requires the Rab11-dependent endocytic recycling pathway. J Infect Dis 218:S388–S396. https://doi.org/10.1093/infdis/jiy460
50. Nanbo A, Watanabe S, Halfmann P, Kawaoka Y. 2013. The spatio-temporal distribution dynamics of Ebola virus proteins and RNA in infected cells. Sci Rep 3:1206. https://doi.org/10.1038/srep01206
51. Nanbo A, Maruyama J, Imai M, Ujie M, Fujioka Y, Nishide S, Takada A, Ohba Y, Kawaoka Y. 2018. Ebola virus requires a host scramblase for externalization of phosphatidylserine on the surface of viral particles. PLoS Pathog 14:e1006848. https://doi.org/10.1371/journal.ppat.1006848
52. de Castro Martin IF, Fournier G, Sachse M, Pizarro-Cerda J, Risco C, Naffakh N. 2017. Influenza virus genome reaches the plasma membrane via a modified endoplasmic reticulum and Rab11-dependent vesicles. Nat Commun 8:1396. https://doi.org/10.1038/s41467-017-01557-6
53. Ren M, Xu G, Zeng J, De Lemos-Chiarandini C, Adesnik M, Sabatini DD. 1998. Hydrolysis of GTP on rab11 is required for the direct delivery of transferrin from the pericentriolar recycling compartment to the cell surface but not from sorting endosomes. Proc Natl Acad Sci U S A 95:6187–6192. https://doi.org/10.1073/pnas.95.11.6187
54. Gromov PS, Celis JE, Hansen C, Tommerup N, Gromova I, Madsen P. 1998. Human rab11a: transcription, chromosome mapping and effect on the expression levels of host GTP-binding proteins. FEBS Lett 429:359–364. https://doi.org/10.1016/S0014-5793(98)00607-3
55. Silvis MR, Bertrand CA, Ameen N, Golin-Bisello F, Butterworth MB, Frizzell RA, Bradbury NA. 2009. Rab11b regulates the apical recycling of the cystic fibrosis transmembrane conductance regulator in polarized intestinal epithelial cells. Mol Biol Cell 20:2337–2350. https://doi.org/10.1091/mbc.e08-01-0084
56. Welz T, Wellbourne-Wood J, Kerkhoff E. 2014. Orchestration of cell surface proteins by Rab11. Trends Cell Biol 24:407–415. https://doi.org/10.1016/j.tcb.2014.02.004
57. Schudt G, Kolesnikova L, Dolnik O, Sodeik B, Becker S. 2013. Live-cell imaging of Marburg virus-infected cells uncovers actin-dependent transport of nucleocapsids over long distances. Proc Natl Acad Sci U S A 110:14402–14407. https://doi.org/10.1073/pnas.1307681110
58. Horgan CP, McCaffrey MW. 2009. The dynamic Rab11-FIPs. Biochem Soc Trans 37:1032–1036. https://doi.org/10.1042/BST0371032
59. Desnos C, Huet S, Darchen F. 2007. "Should I stay or should I go?": myosin V function in organelle trafficking. Biol Cell 99:411–423. https://doi.org/10.1042/BC20070021
60. Horgan CP, Hanscom SR, Jolly RS, Futter CE, McCaffrey MW. 2010. Rab11-FIP3 links the Rab11 GTPase and cytoplasmic dynein to mediate transport to the endosomal-recycling compartment. J Cell Sci 123:181–191. https://doi.org/10.1242/jcs.052670

61. Matsuzaki F, Shirane M, Matsumoto M, Nakayama KI. 2011. Protrudin serves as an adaptor molecule that connects KIF5 and its cargoes in vesicular transport during process formation. Mol Biol Cell 22:4602–4620. https://doi.org/10.1091/mbc.e11-01-0068
62. Schonteich E, Wilson GM, Burden J, Hopkins CR, Anderson K, Goldenring JR, Prekeris R. 2008. The Rip11/Rab11-FIP5 and kinesin II complex regulates endocytic protein recycling. J Cell Sci 121:3824–3833. https://doi.org/10.1242/jcs.032441
63. Oda S, Noda T, Wijesinghe KJ, Halfmann P, Bornholdt ZA, Abelson DM, Armbrust T, Stahelin RV, Kawaoka Y, Saphire EO. 2016. Crystal structure of Marburg virus VP40 reveals a broad, basic patch for matrix assembly and a requirement of the N-terminal domain for immunosuppression. J Virol 90:1839–1848. https://doi.org/10.1128/JVI.01597-15
64. Bornholdt ZA, Noda T, Abelson DM, Halfmann P, Wood MR, Kawaoka Y, Saphire EO. 2013. Structural rearrangement of Ebola virus VP40 begets multiple functions in the virus life cycle. Cell 154:763–774. https://doi.org/10.1016/j.cell.2013.07.015
65. Adu-Gyamfi E, Digman MA, Gratton E, Stahelin RV. 2012. Investigation of Ebola VP40 assembly and oligomerization in live cells using number and brightness analysis. Biophysical Journal 102:2517–2525. https://doi.org/10.1016/j.bpj.2012.04.022
66. Han Z, Harty RN. 2005. Packaging of actin into Ebola virus VLPs. Virol J 2:92. https://doi.org/10.1186/1743-422X-2-92
67. Kolesnikova L, Ryabchikova E, Shestopalov A, Becker S. 2007. Basolateral budding of Marburg virus: VP40 retargets viral glycoprotein GP to the basolateral surface. J Infect Dis 196:S232–S236. https://doi.org/10.1086/520584
68. Albariño CG, Uebelhoer LS, Vincent JP, Khristova ML, Chakrabarti AK, McElroy A, Nichol ST, Towner JS. 2013. Development of a reverse genetics system to generate recombinant Marburg virus derived from a bat isolate. Virology 446:230–237. https://doi.org/10.1016/j.virol.2013.07.038
69. Miller MR, McMinn RJ, Misra V, Schountz T, Müller MA, Kurth A, Munster VJ. 2016. Broad and temperature independent replication potential of filoviruses on cells derived from old and New World bat species. J Infect Dis 214:S297–S302. https://doi.org/10.1093/infdis/jiw199
70. Nanbo A, Imai M, Watanabe S, Noda T, Takahashi K, Neumann G, Halfmann P, Kawaoka Y. 2010. Ebolavirus is internalized into host cells via macropinocytosis in a viral glycoprotein-dependent manner. PLoS Pathog 6:e1001121. https://doi.org/10.1371/journal.ppat.1001121